Materials
Advances

ROYAL SOCIETY
OF CHEMISTRY

REVIEW

View Article Online
View Journal | View Issue

Cite this: *Mater. Adv.*, 2023, 4, 787

Homoconjugation effects in triptycene based organic optoelectronic materials

Jai-Ram Mistry, Stephanie Montanaro and Iain A. Wright *†

Received 10th May 2022,
Accepted 4th January 2023

DOI: 10.1039/d2ma00523a

rsc.li/materials-advances

Molecular size and shape have a commanding influence on the electronic structure and photophysical properties of organic optoelectronic molecules. Small changes in, for example, the dihedral angles between two rings in a molecule can be used to fine tune frontier orbital distributions, and make the difference between efficient or poor absorbance, luminescence, charge transport *etc.* as well as impacting on mechanical and thermal properties to improve processability. Recent works have made it clear that structural changes which enforce homoconjugation, the through-space overlap of frontier π-orbitals across a shared non-conjugating group, can exert even more dramatic changes on these useful functional properties. Triptycene is an archetypical homoconjugated molecule with a rigid 3D structure which presents an ideal substrate from which to learn how best to employ homoconjugation to optimise functional molecular properties. This review demonstrates this by highlighting triptycene-based molecules in the context of organic electronic materials, where homoconjugation has resulted in markedly enhanced optoelectronic properties, and provides comment on the performance and future potential of these materials in devices where possible.

Introduction

Triptycene is a classic 3D polycyclic aromatic hydrocarbon with a paddlewheel-like structure. It consists of three benzene "fins" bound *via* two shared sp^3 bridgehead carbon atoms (structure shown in Fig. 1). This rigid structure has led to extensive study in applications including molecular gears,[1,2] motors[3,4] and nanovehicles,[5,6] sensors,[7,8] porous polymers for gas separation,[9–11] photocatalysis,[12–15] chiral luminescent polymers,[16,17] and as a key structural component of both metal[18,19] and covalent organic frameworks[20] and polymer networks.[21] The large internal free volume between the fins of triptycene has also been exploited to control morphology and solubility in polymers and thin films.[22–27] The fins of triptycene can be readily functionalised which presents great scope for tuning of properties. While this has perhaps been most frequently been encountered as a means to exert further control over morphology in the solid state, using substituents to impart desirable optoelectronic functionality has become an increasingly visible aspect of modern triptycene chemistry as will be highlighted throughout this review.

Homoconjugation in triptycene

An important characteristic of triptycene is that electronic communication can take place between the aryl fins through homoconjugation. IUPAC defines homoconjugation as

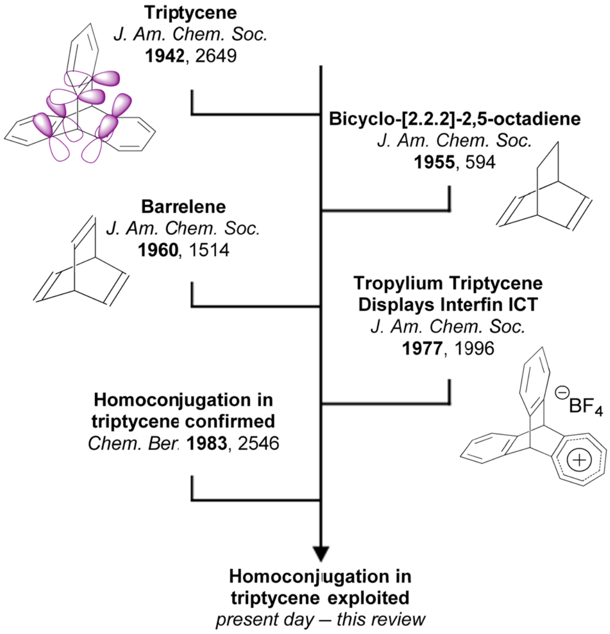

Fig. 1 A short history of homoconjugation in triptycene.

Department of Chemistry, Loughborough University, Loughborough, Leicestershire, LE11 3TU, UK

† Present address: School of Chemistry, University of Edinburgh, Joseph Black Building, David Brewster Road, Edinburgh, EH9 3FJ, UK. E-mail: iain.wright@ed.ac.uk

"*The orbital overlap of two π-systems separated by a non-conjugating group, such as CH_2.*"[28] While homoconjugation may arise in a number of structural tropes,[29] in triptycene it is largely mediated by the transannular, through-space overlap of the π-electron clouds over the aryl fins.

A short history of milestones in understanding homoconjugation in triptycene is illustrated in Fig. 1. Following Bartlett's initial synthesis of triptycene in 1942[30] the possibility of electron transfer between the aryl fins was used to explain the differences between the UV/vis spectra of triphenylmethane and triptycene.[31] The pursuit of homoconjugation underpinned the design and synthesis in 1955 of bicyclo-[2.2.2]-2,5-octadiene[32] and in 1960 of bicyclo-[2.2.2]-octatriene[33] which was given the informal name "barrelene" due to the barrel-like distribution of its frontier orbital density. Confirmation of homoconjugation in barrelene[34–37] led to renewed interest in identifying homoconjugation effects in triptycene. As triptycene has a barrelene core it seemed intuitive that through-space electronic interactions should be occurring, but as the π-electrons in barrelene are olefinic and those in triptycene are benzenoid, the influence of any transannular interactions in triptycene remained contentious. In 1977 a triptycene bearing one cationic tropylium tetrafluoroborate fin demonstrated clear intramolecular charge transfer (ICT) character in its UV/vis spectrum which could only arise from electron transfer between fins.[38] Homoconjugation in triptycene was finally proven using ultraviolet photoelectron spectroscopy in the early 1980s.[39,40] Recent articles from the Mastalerz group which provides both reference to other key articles that led to this conclusion, alongside further experimental evidence of homoconjugation in triptycene derivatives.[41,42]

Since these studies, numerous other molecules were synthesised which clearly displayed the influence of homoconjugation, however it is only in recent years that this phenomenon has begun to be employed deliberately to exert control over the photophysical and electrochemical properties of triptycenes for optoelectronic applications. This review will focus on homoconjugation effects in triptycenes in this context. Following a short description of how to identify and modulate homoconjugation, the rest of this review consists of sections concerning organic light emitting devices (OLEDs), organic solar cells (OSCs) and charge transport/storage technologies. Specific comments will be made towards identifying the influence (or not) of homoconjugation on photophysical or electrochemical properties with the aim of obtaining a clearer picture of how best to utilise this effect in future materials development.

Observing and controlling homoconjugation in triptycene

Studies by the Rathore group provide some of the clearest pictures for identifying and understanding the influence of homoconjugation on the electronic properties of triptycene by simple visual analysis of the results of DFT calculations.[43,44] A larger amount of frontier orbital density at the core of the triptycene indicates that stronger electronic coupling between the fins can be expected.

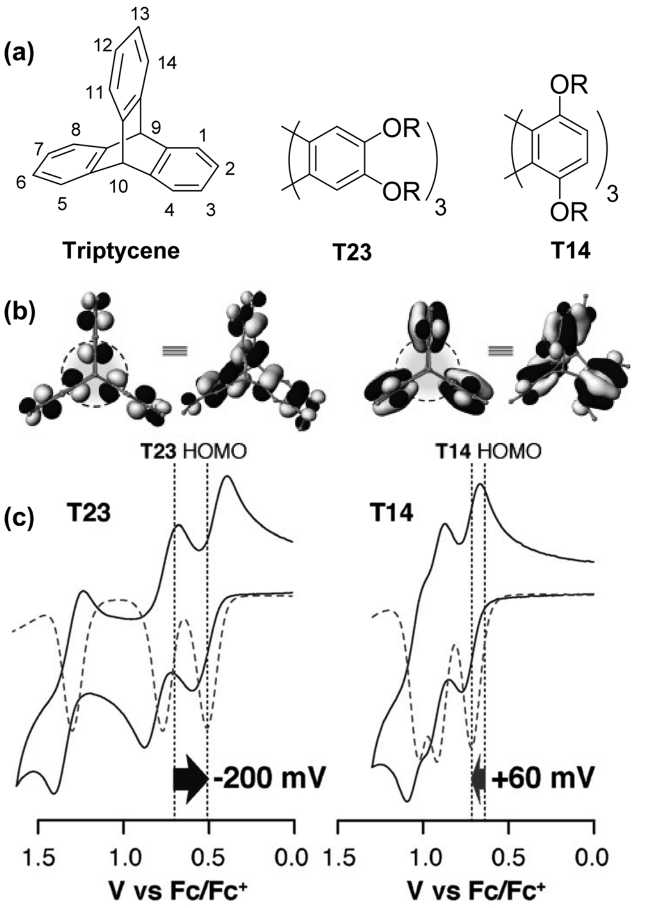

Fig. 2 (a) Molecular structure of triptycene and alkoxy substituted triptycenes **T23** and **T14**; (b) molecular orbital profiles for **T23** and **T14**; (c) cyclic voltammograms for **T23** and **T14**. Reproduced with permission from ref. 43. Copyright 2015, Wiley-VCH.

In an elegant demonstration of this, they studied the influence of the regiochemistry of electron-donating alkoxy –OR substituents on the electronic structure of substituted triptycenes **T23** and **T14** using computational and electrochemical methods (Fig. 2a–c). In Fig. 2b it is clear that when the –OR groups are on the 1,4,5,8,11,14-*peri*-sites of triptycene in **T14** there is more limited distribution of the HOMO over the triptycene core compared to when the –OR substituents are *para*- to the benzylic 9,10-bridgehead carbon atoms in the 2,3,6,7,12,13-positions in **T23**. This results in reduced transannular overlap and thereby diminished influence of homoconjugation in the HOMO manifold for **T14**. The consequences of this are directly observable in the electrochemical properties of **T23** and **T14** as shown in Fig. 2c. Both molecules display three sequential single-electron oxidation events corresponding to the concomitant oxidation of each fin. While for **T23** three distinct and well-separated oxidation waves were observed, greatly reduced separation of these oxidations was observed for **T14** demonstrating the more limited electronic coupling between fins arising from this substitution pattern.

As well as impacting on electrochemical behaviour, it is becoming increasingly clear that homoconjugation in triptycene derivatives can lead to increases in optical properties such as photoluminescence quantum yields (PLQY), molar extinction coefficients (ε) and oscillator strengths (f_{osc}). These super-summative increases are greater than the threefold enhancement that might be expected in the absence of any electronic communication between the arms of the triptycene (*vide infra*).

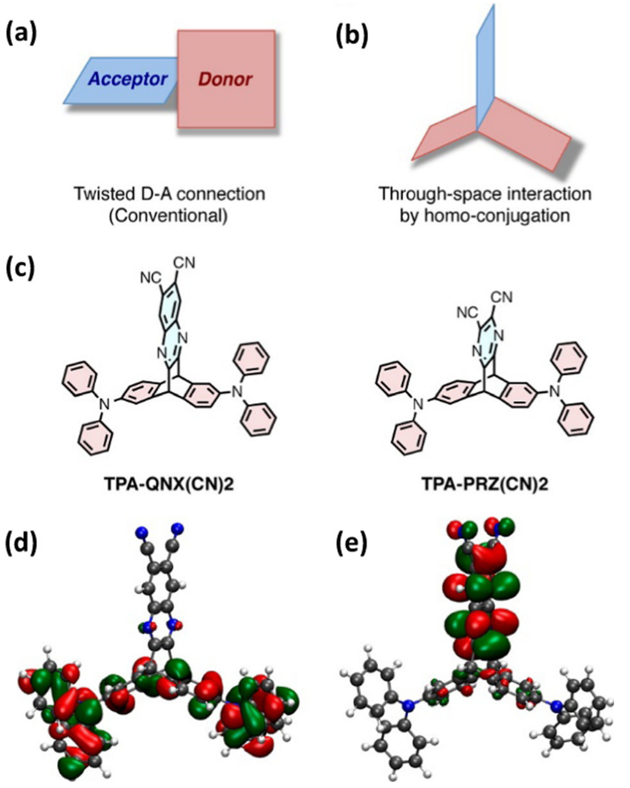

Fig. 3 (a) Traditional and (b) homoconjugated TADF design strategy employed in ref. 45. (c) Chemical structures of **TPA-QNX(CN)2** and **TPA-PRZ(CN)2** and the (d) HOMO and (e) LUMO of **TPA-QNX(CN)2**. Adapted with permission from ref. 45. Copyright 2015, American Chemical Society.

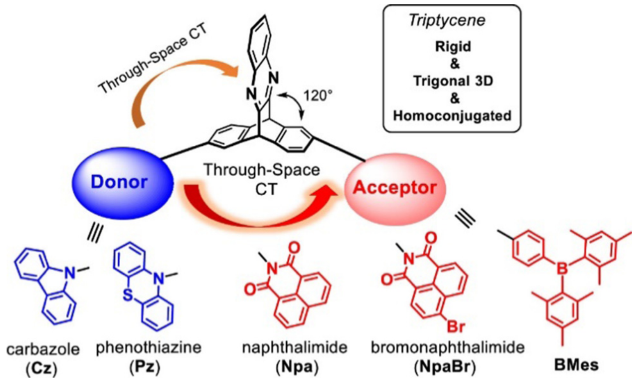

Fig. 4 Molecular structures of compounds studied in ref. 47. Copyright 2020, American Chemical Society.

Homoconjugated triptycene luminophores for OLEDs

In 2015 an initial effort to use homoconjugation to produce thermally activated delayed fluorescent (TADF) molecules was published by Kawasumi *et al.*[45] TADF is an emission mechanism which, at a basic level, relies upon a small energy gap between the first excited singlet and triplet states (ΔE_{ST}) facilitating reverse intersystem crossing (rISC) to convert non-radiative triplet states into radiative singlet states.[46] In an OLED device triplets and singlets are formed in a 3 : 1 ratio so using TADF to harvest the triplets which are otherwise lost is a primary pathway to improve device efficiencies.

Taking inspiration from established twisted donor–acceptor (D–A) TADF chromophores (whereby a large dihedral angle is imposed between D and A to ensure orthogonal separation of the HOMO and LUMO and reduce E_{ST}) this work used homoconjugation to facilitate weak orbital overlap and thereby through-space charge transfer (TSCT) between two triphenylamine D fins and a single dicyanoquinoxaline or dicyanopyrazine A fin in the triptycenes **TPA-QNX(CN)2** and **TPA-PRZ(CN)2** (Fig. 3a–c) for which ΔE_{ST} of 111 meV and 75 meV respectively were obtained. In the DFT results (Fig. 3d and e), homoconjugation can be observed over the sp^2 carbon atoms attached to the sp^3 bridgehead carbons. Solution state PLQYs were significantly reduced in the presence of air and a linear relationship between excitation and emission intensity was obtained. These two factors provide strong evidence of TADF. Yellow OLEDs with external quantum efficiencies (EQE) up to 9.4% for **TPA-QNX(CN)2** (4.0% for **TPA-PRZ(CN)2**) were obtained. Homoconjugation therefore proved to be an effective method to facilitate TADF.

A similar design motif was exploited by Lei *et al.* where the acceptor fin was a simple non-functionalised quinoxaline which was used to make luminescent D–A–D and D–A–A systems (Fig. 4). These molecules exploited homoconjugation through the LUMO manifold and tuned the emission wavelengths between 329 and 625 nm by varying the fin-appended donors and acceptors.[47]

A subsequent report from the Swager group in conjunction with Buchwald showed that homoconjugation in a fused indole-triptycene donor **TCZ** used in conjunction with triazole-based acceptors exerted much more subtle control over ΔE_{ST} to improve TADF properties (structures in Fig. 5).[48] The presence of the **TCZ** moiety led to a slight redshift in PL and a 0.03 eV reduction in ΔE_{ST} compared to a simple carbazole analogue. The bulky nature of **TCZ** turned on emission in a film of the molecule doped at 15 wt% into bis[2-(diphenylphosphino)phenyl] ether oxide (DPEPO). OLED devices of **TCZ-TRZ** and **TCZ-TRZ(Me)** had maximum EQE of 10.4 and 11.1% respectively but showed significant efficiency roll-off at 50 cd m^{-2} dropping to EQE = 3.4% and 2.0% due to degradation at high current density.

A short series of ring-fused triptycenes wherein one fin of the triptycene consisted of a coumarin-like moiety was reported by Qian *et al.*[49] **DCT-1** featured a 1,4-dimethoxybenzene donor fin and was shown to undergo a homoconjugation facilitated ICT from this electron-rich fin to the electron-poor coumarin

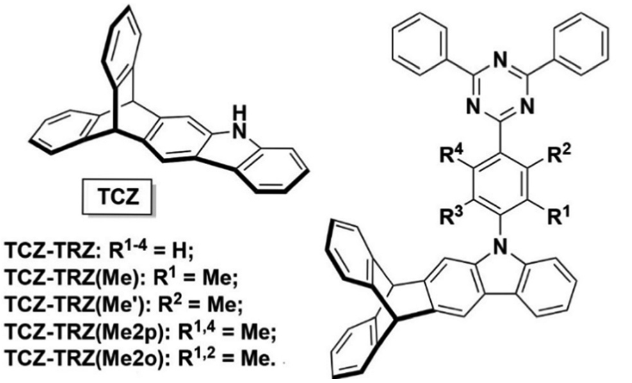

Fig. 5 Donor–acceptor compounds of the **TCZ-TRZ** series from ref. 48 featuring homoconjugation on the periphery of the molecule. Adapted with permission from ref. 48. Copyright 2018, American Chemical Society.

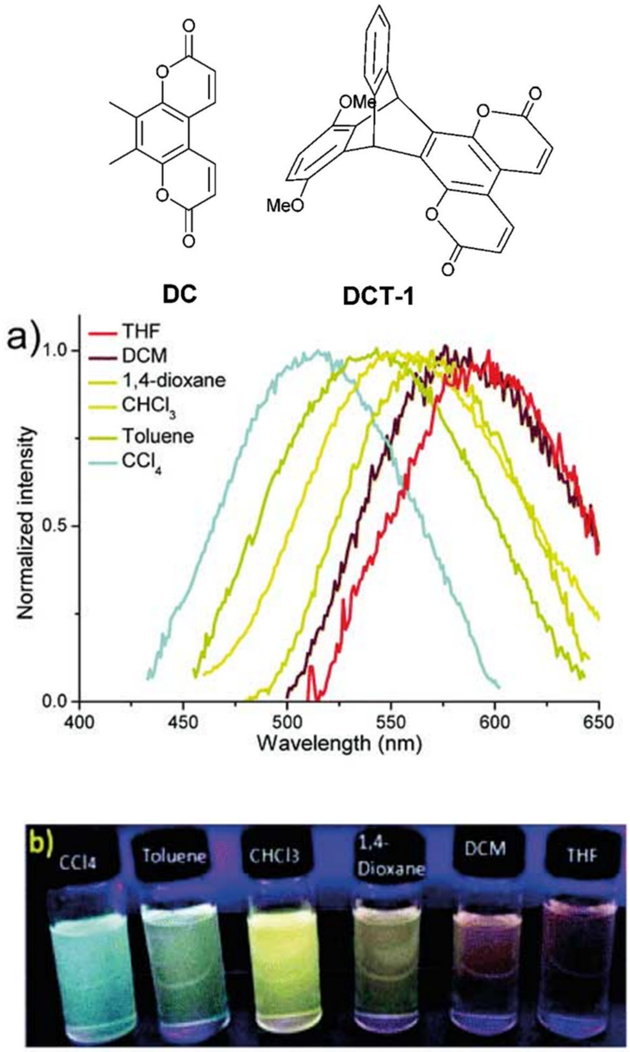

Fig. 6 Coumarin dye **DC** and its homoconjugated ICT analogue **DCT-1** and (a) emission spectra and (b) visual representation of the solvatochromism of **DCT-1**. Reproduced from ref. 49 with permission from the Royal Society of Chemistry.

fin resulting in a charge separated excited state (structures, spectra and visual responses shown in Fig. 6). This was confirmed by the observation of positive solvatochromism and corroborated by computational insights. While the PLQY in solution was generally low, especially in comparison to the non-ICT compound, the donor–acceptor molecule displayed aggregation induced emission (AIE). The AIE was attributed to the methoxy groups hindering fin to fin stacking which leads to aggregation-caused quenching for the other molecules.

In 2019 Montanaro *et al.* presented a pyrazine fused D–π–A triptycene **3CzQ** featuring six 3,6-di-*tert*-butylcarbazole donors bound to an electron poor pyrazine fused triptycene core through 1,4-phenylene spacers.[50] In contrast with the ICT molecules discussed above where homoconjugation has facilitated TSCT between electron-rich and -poor fins, the structural motif of **3CzQ** results in through-bond charge transfer (TBCT) from the donor carbazoles into the homoconjugated acceptor triptycene core. To fully evaluate the impact of this structure, the properties of **3CzQ** were presented in comparison with a single-fin analogue **CzQ** (structures shown in Fig. 7).

Cyclic voltammetry supported by DFT revealed that the HOMO is distributed uniformly over the carbazole heterocycles while the LUMO is sequestered in the homoconjugated tris(quinoxline) core. The absence of significant communication between the carbazole rings of **3CzQ** was evidenced by a simultaneous and reversible three-electron oxidation of the triptycene compared to the reversible single-electron oxidation observed for the single fin.

The D–π–A structure gave rise to intense ICT bands in the absorption and emission spectroscopy of both molecules (Fig. 8a and Table 1). Both also displayed blue emission with the emission maximum of the triptycene slightly red-shifted (5 nm) compared to the single fin. Due to a narrower photoluminescence full width at half maximum the Commission Internationale de L'Eclairage (CIE) coordinates of the molecules are nearly identical so colour purity remains unaffected.

An important observation from this study is that a near five-fold enhancement in extinction coefficient was observed for **3CzQ** *vs.* **CzQ** alongside a 37.5% increase in PLQY (Table 1). In contrast with the TSCT systems, TBCT is occurring from the carbazole donors into the homoconjugated tris(quinoxaline) core. TDDFT calculations revealed multiple low-lying excited states which led to a four-fold enhancement in the ICT oscillator strength **3CzQ** over **CzQ**. This is seemingly a direct consequence of the high symmetry homoconjugated structure. Limited oxygen sensitivity was observed in the PLQY of both molecules which indicated that a triplet mediated emission process may also be at play.

The enhancement in PLQY, its apparent sensitivity to oxygen and the multiple low-lying excited states which were observed for **3CzQ** presents an intriguing avenue to explore towards TADF. As described at the start of this section, TADF relies upon a narrow ΔE_{ST} to induce rISC, and efficient rISC is also dependent upon spin–orbit coupling between states. This is realised by having multiple partially delocalised triplet states with both locally-excited and charge transfer character.[51–53] **3CzQ** satisfies the last of these criteria well but TADF was not

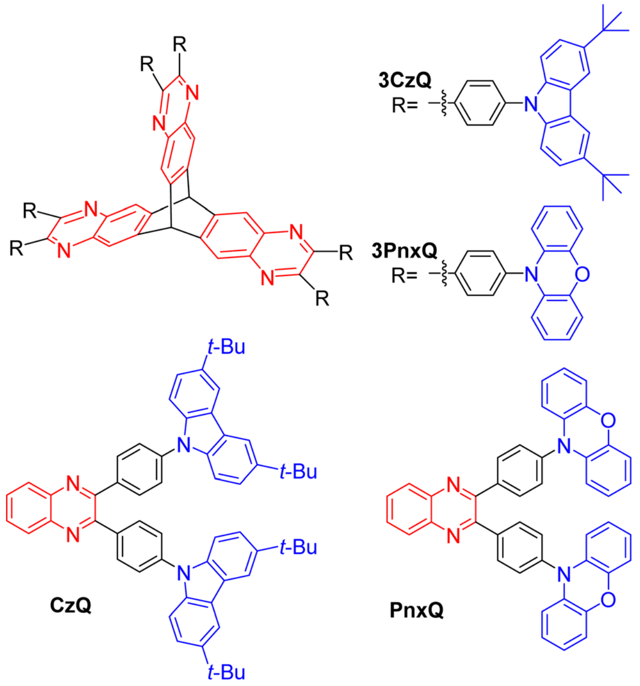

Fig. 7 Molecular structures of triptycenes **3CzQ** and **3PnxQ** and their single fin analogues **CzQ** and **PnxQ**.

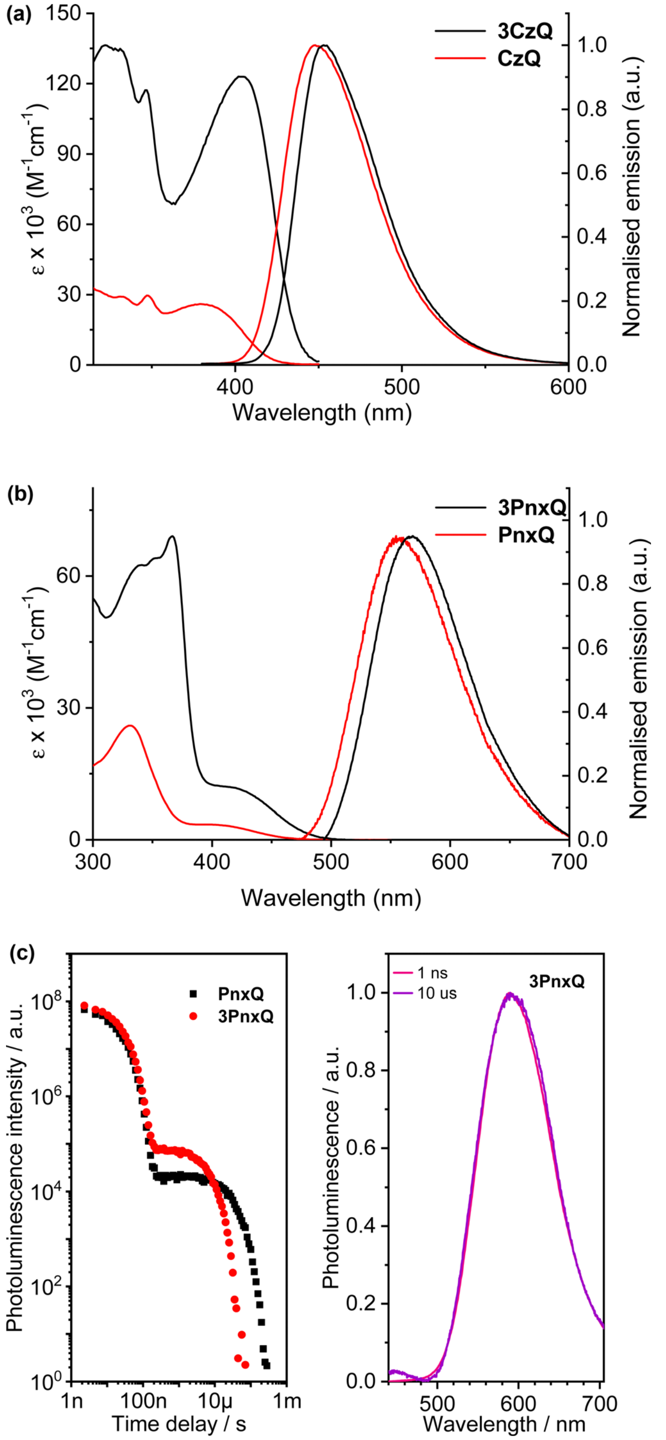

Fig. 8 Absorption and normalised emission spectra of (a) **3CzQ** and **CzQ**; (b) **3PnxQ** and **PnxQ**; (c) photoluminescence decay of **PnxQ** and **3PnxQ** (left) and prompt and delayed time-resolved spectra for **3PnxQ** (right).

observed, likely due to ΔE_{ST} being too large. By adopting a different donor ΔE_{ST} can be reduced at which point the multiple excited states facilitated by the homoconjugated iptycene will serve to enhance rISC while the super-summative increases in ε and f_{osc} should maintain strong emission. These two properties are usually offset by one another so improving both simultaneously is a very desirable outcome.

By changing the donor moiety of **3CzQ** from carbazole to the stronger donor phenoxazine **3PnxQ** was realised and displayed a narrower ΔE_{ST}.[54] The analogous single-fin **PnxQ** is a known TADF luminophore[55] which was re-synthesised to permit direct comparison and validation against a known compound, the structures of both are shown in Fig. 7. Large improvements of ε and f_{osc} were again observed for **3PnxQ** alongside clear TADF emission (Fig. 8b and c, Table 1). Computational results indicated much stronger spin–orbit coupling for **3PnxQ** over **PnxQ** and greatly increased f_{osc} for $S_0 \rightarrow S_1$ and $S_0 \rightarrow S_2$. The homoconjugated structure successfully demonstrated a 250% acceleration in k_{rISC} in toluene solution and almost 100% in a solution processed **3PnxQ** doped (concentration 5 wt%) PVK:PBD thin film. OLED devices of **3PnxQ** in PVK:PBD showed better performance overall than those of **PnxQ**, particularly in terms of maximum luminance (14.8×10^3 cd m^{-2} for **3PnxQ**; 8.9×10^3 cd m^{-2} for **PnxQ**) and charge density (220 mA cm^{-2} for **3PnxQ**; *vs.* 120 mA cm^{-2} for **PnxQ**).

Homoconjugated triptycene chromophores for OSCs

In 2013 a theoretical study by Liu and Troisi highlighted that low-lying and degenerate excited states in fullerene were responsible for their reliably high performance in bulk heterojunction (BHJ) OSCs.[56] They demonstrated computationally that the use of methine bridges, in other words homoconjugation, between chromophores would serve to create the degeneracy required. Yang *et al.* also performed DFT analysis of ladder-type NFA moieties fused to a triptycene core.[57] This

Table 1 Summary of ICT wavelength absorbance and emission properties for **CzQ**, **3CzQ**, **PnxQ** and **3PnxQ**

	λ_{abs} (nm) [$\varepsilon \times 10^3$ M^{-1} cm^{-1}]	$\lambda_{\text{max PL}}$ (nm)	PLQY (%)
CzQ	383 (26)	448	35
3CzQ	402 (123)	453	56
PnxQ	398 (3.5)	574	50
3PnxQ	420 (12)	583	61

revealed LUMO degeneracy and homoconjugation in the HOMO. The calculations predict that more excitons will be generated from the triptycene and that the exciton binding energy is notably smaller for the 3D material due to reduced coulombic attraction. Triptycene therefore presents a promising scaffold from which to try and emulate useful properties of fullerene.

A report in 2016 from the Mastalerz group was among the first to explore these findings in tandem with harnessing homoconjugation effects.[58] They produced isomeric ring-fused triptycenes with electron-accepting aroylenimidazole fins ***C*$_{3\text{V}}$-D-TTAI** and ***C*$_\text{S}$-D-TTAI** (Fig. 9a). The isomers displayed similar optoelectronic properties (spectra shown in Fig. 9b) and comparable performance in BHJ devices. These molecules have optical band gaps (E_g) of 2.2 eV and $\varepsilon \sim 16 \times 10^3$ M^{-1} cm^{-1} for the lowest energy absorption band and emit orange-red light at 622 nm with a PLQY of 10–12%. While the low energy band was not formally assigned as an ICT transition, DFT results (Fig. 10) indicated that the HOMO is sited primarily over the triptycene moiety of these molecules while the LUMO and LUMO+1 are degenerate and distributed widely over the fins. This observation, alongside the absence of any of the fine-structure observed in the absorbance and emission spectra of related naphthalene diimide chromophores,[59] makes some CT character seem likely. The frontier orbital distribution contrasts with the molecules **3CzQ** and **3PnxQ** mentioned in the previous section, where the frontier orbitals of the LUMO manifold are densely localised over the triptycene core while the HOMO is spread over the peripheral donors.

BHJ OSCs of **2a**-**b** fabricated with poly(3-hexylthiophene) (**P3HT**) had open circuit voltages (V_{oc}) of 0.50 V and fill factors (FF) of 0.36 to 0.39 alongside short circuit currents (J_{sc}) to the order of 1 mA cm^{-2} were obtained. The low J_{sc} was attributed primarily to the poor morphology of the BHJ. The use of the more strongly electron donating polymer **PTB7** increased both V_{oc} and J_{sc} thereby improving the power conversion efficiency (PCE) to 1%.

To help overcome solubility issues encountered in the initial study the R-groups of the terminal diimides were changed from 2,6-di-iso-propylphenyl to 2-ethylhexyl (***C*$_{3\text{V}}$-E-TTAI** and ***C*$_\text{S}$-E-TTAI**) and 9-heptadecyl chains (***C*$_{3\text{V}}$-B-TTAI** and ***C*$_\text{S}$-B-TTAI**).[60] The authors comment that the optical properties of the molecules do not vary upon changing the side chain groups, and indeed there is minimal change in the overall profile of the absorbance or the ultraviolet photoemission spectra (Fig. 11). However the absorbance data suggests there are significant increases in ε upon moving from an aryl to an alkyl solubilising group (Table 2).

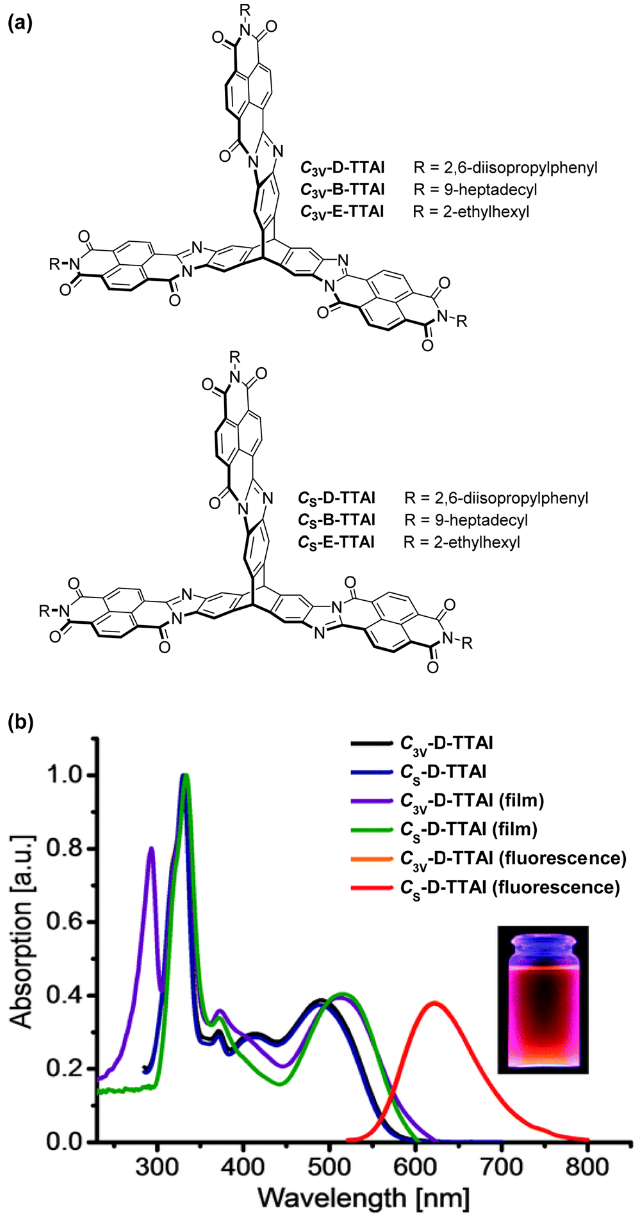

Fig. 9 (a) Molecular structures of triptycene-trisaroylenimidazoles; (b) CH_2Cl_2 solution absorbance and emission spectra and thin film absorbance spectra of ***C*$_{3\text{V}}$-D-TTAI** and ***C*$_{3\text{V}}$-D-TTAI**. Reproduced from ref. 58 with permission from the Royal Society of Chemistry.

In BHJ OSC with **PTB7** the *N*-alkyl **E** and **B** analogues greatly outperformed the *N*-aryl **D** molecules, demonstrating an approximately threefold enhancement in PCE in all cases, primarily due to large increases in J_{SC}. A maximum PCE of 3.16% was observed for ***C*$_\text{S}$-E-TTAI** in a 1 : 1 D : A device. The devices still suffered from losses due to bimolecular recombination. Interestingly, the 2-ethylhexyl bearing molecules had a lower V_{oc} than those bearing 9-heptadecyl chains despite having essentially identical frontier orbital energies. This variation in V_{oc} was assigned to an improved microstructure in the BHJ. The 2-ethylhexyl bearing molecules also had improved J_{sc} over

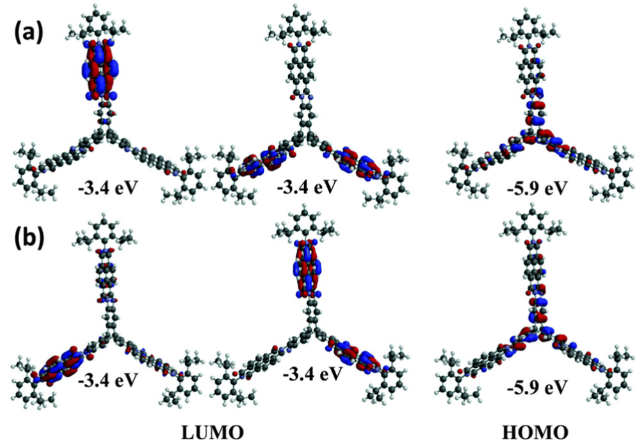

Fig. 10 DFT-calculated frontier orbitals for (a) **C_S-D-TTAI** and (b) **C_{3V}-D-TTAI**. Reproduced from ref. 58 with permission from the Royal Society of Chemistry.

Table 2 Summary of longest wavelength absorbance and emission characteristics for **1a–c**, **2a–c**, and the **TDAI** and **TTAI** series of acceptors

	λ_{abs} (nm) [$\varepsilon \times 10^3$ M^{-1} cm^{-1}]	$\lambda_{max\,PL}$ (nm)
1a	440 (19.9)	569
1b	435 (19.9)	561
1c	442 (19.9)	565
2a	324 (25.1), 476 (10.0)	624
2b	324 (50.1), 476 (19.9)	620
2c	323 (31.6), 476 (12.6)	620
C_2-B-TDAI	328 (63.1), 483 (25.1)	615
C_2-E-TDAI	328 (50.1), 483 (15.8)	615
C_S-B-TDAI	328 (63.1), 483 (25.1)	615
C_S-E-TDAI	328 (63.1), 483 (19.9)	615
C_{3V}-D-TTAI	329 (48.2), 486 (16.5)	620
C_S-D-TTAI	331 (50.1), 490 (15.8)	618
C_{3V}-B-TTAI	329 (158), 484 (50.1)	620
C_{3V}-E-TTAI	329 (126), 484 (50.1)	616
C_S-B-TTAI	329 (199), 484 (63.1)	620
C_S-E-TTAI	329 (126), 484 (50.1)	620

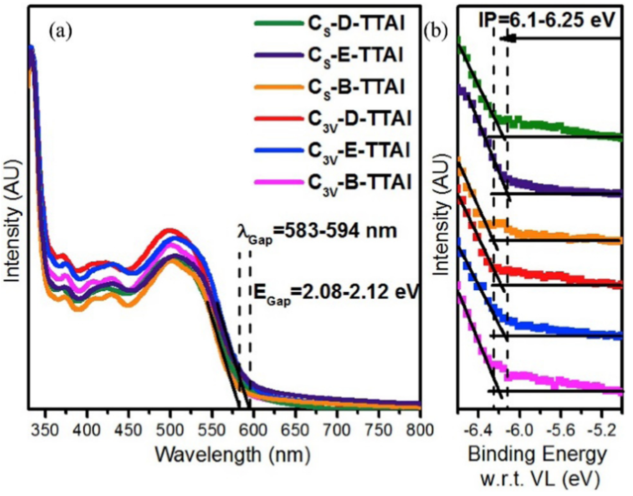

Fig. 11 (a) Absorbance spectra of the **TTAI** acceptors and; (b) their ultraviolet photoemission spectroscopy indicating limited change in ionisation potential (IP). Reproduced with permission from ref. 60. Copyright 2017, Elsevier.

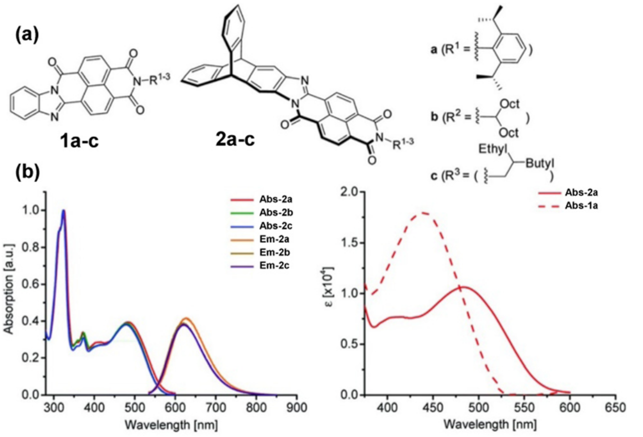

Fig. 12 (a) Molecular structures of **1a–c** and **2a–c**. (b) Left: Absorbance and emission spectra of **2a–c**. Right: Comparison of longest wavelength absorbance of **1a** and **2a**. Reproduced from ref. 61 with permission from the Chinese Chemical Society (CCS), Shanghai Institute of Organic Chemistry (SIOC), and the Royal Society of Chemistry.

the 9-heptadecyls and therefore marginally outperformed them overall.

Subsequent papers systematically provided the properties of single fins **1a–c**, single-finned triptycenes **2a–c** (Fig. 12a)[61] and two pairs of isomeric double-finned triptycenes **C_2-B-TDAI** and **C_2-E-TDAI** and **C_S-B-TDAI** and **C_S-E-TDAI** (Fig. 13a) where **B** indicates R = 9-heptadecyl and **E** indicates R = 2-ethylhexyl.[62] For the triptycene containing **2a–c**, similar frontier orbital distributions to **$C_{3V/S}$-D-TTAI** were calculated with the HOMO localised over the triptycene core and the LUMO spread over the electron poor fins. Degenerate LUMO and LUMO+1 were again predicted for **$C_{2/S}$-B/E-TDAI.** The non-triptycene single fins **1a–c** have larger ε for the longest wavelength absorbance peak compared to **2a–c**, but significantly blue-shifted absorbance (Fig. 12b). The profile of the absorbance and emission spectra of the single-finned **2a–c** and double-finned **TDAI** compounds (Fig. 13b) are very similar to those of the triple-finned **TTAI** series but the triple-finned systems retain the highest ε.

Generally, the optical properties of the two-finned triptycenes are not improved compared to the single-finned triptycenes. They show slight enhancements in the intensity of both the highest and lowest energy bands alongside a slight blue-shift in emission and narrowing of the Stokes shift. Upon moving to a three-finned system, super-summative enhancements in both the highest and lowest energy bands are observed when comparing one to three fins for the **B-** and **E-TTAI** triptycenes. The clearest example of this is in the 2-ethylhexyl series where **C_{3V}-E-TTAI** and **C_S-E-TTAI** display a 4-fold enhancement in both the high and low energy bands compared to **2c**.

While OSC performance remains modest, the presence of the triptycene moiety did lead to a higher PCE of 2.2% for **2a**

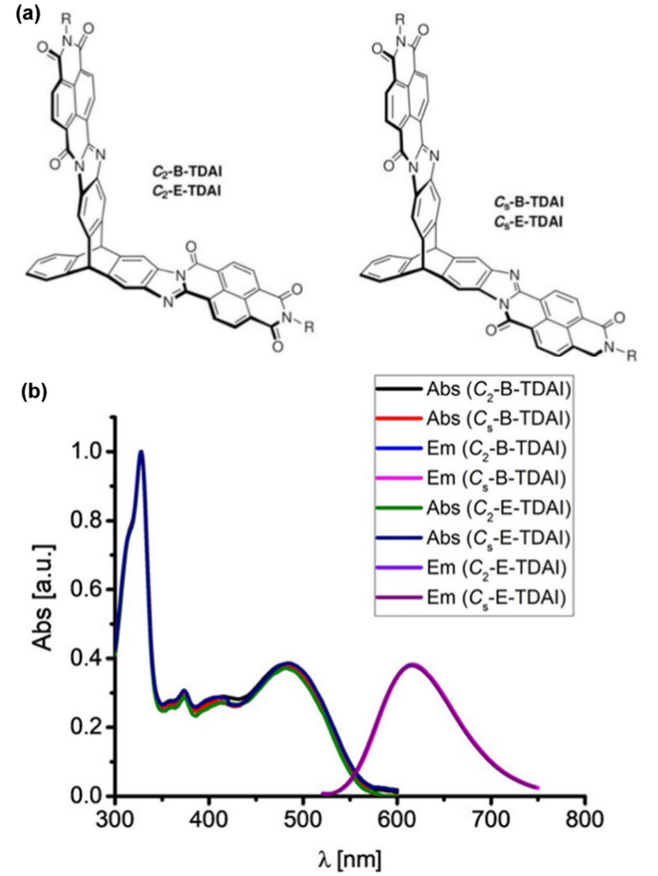

Fig. 13 (a) Molecular structures of **$C_{S/2}$-B/E-TDAI**; (b) solution absorbance and emission spectra for **$C_{S/2}$-B/E-TDAI**. Adapted with permission from ref. 62. Copyright 2017, Wiley-VCH.

with **PTB7** as donor (compared to 1.2% for **1a**). Low FF (<42%) were observed in all devices. The double-finned triptycenes performed similarly in OSCs with **$C_{S/2}$-B-TDAI** displaying PCE of ∼2% and **$C_{S/2}$-E-TDAI** displaying PCE of ∼1%.

Other imide-based acceptors that have been employed with triptycene in a similar fashion are useful to make comparisons of. Perylene-3,4,9,10-tetracarboxylic acid diimides (**PDIs**) are an established class of NFA material. **PDI** is a planar molecule with a strong tendency to aggregate due to π–π stacking interactions which is a limiting factor in its utility.[63] While imposing twists between adjacent **PDI** units has previously been used to overcome this,[64,65] Liu *et al.* chose to exploit the internal free-volume of triptycene to hinder aggregation between electron accepting **PDI** fragments.[66] Suzuki cross-coupling between a triptycene 2,7,14-tris(boronate) ester and a 1-bromo**PDI** bearing R = 2-octyldodecyl produced the molecule **TP3** (Fig. 14). This greatly improved solubility and reduced aggregation.

Degeneracy was observed in the frontier orbital manifolds as predicted by computational methods. The HOMO and LUMO manifolds were distributed almost exclusively across the pendant **PDI** units with only limited density over the triptycene. Experimentally, this was reflected in the electrochemistry where all three **PDI** moieties are reduced simultaneously, and in the UV-vis spectrum which has fine structure characteristic of **PDI** and a molar extinction coefficient (ε = 9.4 × 10^4 M^{-1} cm^{-1} at 540 nm in $CHCl_3$) which shows only slight enhancement over unfunctionalised *N*,*N*′-bis(2-ethylhexyl)**PDI** molecules (ε ∼ 7 × 10^4 M^{-1} cm^{-1} at 525 nm in $CHCl_3$ and ε ∼ 8.5 × 10^4 M^{-1} cm^{-1} at 525 nm in CH_2Cl_2).[67,68]

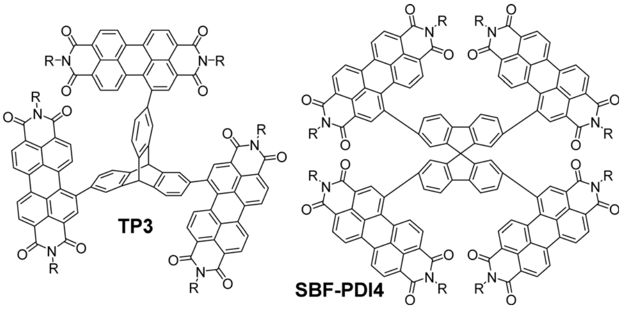

Fig. 14 Molecular structures of non-ring-fused **PDI** functionalised **TP3** (R = 2-octyldodecyl) and its spirocyclic **SBF-PDI4** (R = 2-ethylhexyl).

This study is useful to highlight as it permits comparison with the spirocyclic analogue **SBF-PDI4** (Fig. 14) which has also been studied as the donor in BHJ devices.[69] Spirobifluorene represents another class of 3D hydrocarbon featuring a homoconjugated sp^3 carbon atom.[70,71] The optical properties of **SBF-PDI4** (ε = 9.3 × 10^4 M^{-1} cm^{-1} at 535 nm in $CHCl_3$) are essentially identical to those of **TP3**, and the MO layout is similar. For these molecules, we can conclude that the triptycene or spirobifluorene core is acting as a simple scaffold and not contributing in any meaningful sense to interchromophore coupling. As such, the **PDI** chromophores are acting independently of each other with excitations occurring over rather than between fins.

TP3 was employed in BHJ devices with the polymer **PTB7-Th** displaying PCE up to 3.16%, FF = 0.39 and V_{oc} = 0.86 V and J_{sc} up to 9.54 mA cm^{-2} with the best performing device requiring 0.5 wt% 1,8-diiodooctane (DIO) as an additive. Low FF were observed in all devices. Electron and hole mobility measured using SCLC methods were also low (10^{-4} cm^2 V^{-1} s^{-1}) albeit well-balanced. These poor attributes were ascribed to morphology issues with aggregation and phase separation still occurring despite the large IFV of the triptycene. For **SBF-PDI4** a 1 : 1 D : A device with **PTB7-Th** as donor had near identical performance characteristics to those of **TP3** other than the FF which was improved to 0.48. This indicates that a better heterojunction morphology is obtained using the spirocycle and, importantly, that the configuration of a 3D core can be optimised to improve device performance. The synthesis of **SBF-PDI4** was also published independently by Lee *et al.* and incorporated in devices with polymers **P4T2FBT** and **PV4T2FBT**, obtaining PCE = 5.98% with the latter.[72]

An analogue of **TP3** with smaller solubilising R groups (R = 6-undecyl) was presented in a separate study as an intermediate in the synthesis of the ring fused molecule **T-3**.[73] Single (**T-1**) and double (**T-2**) **PDI** finned analogues were also prepared (structures and absorbance spectra shown

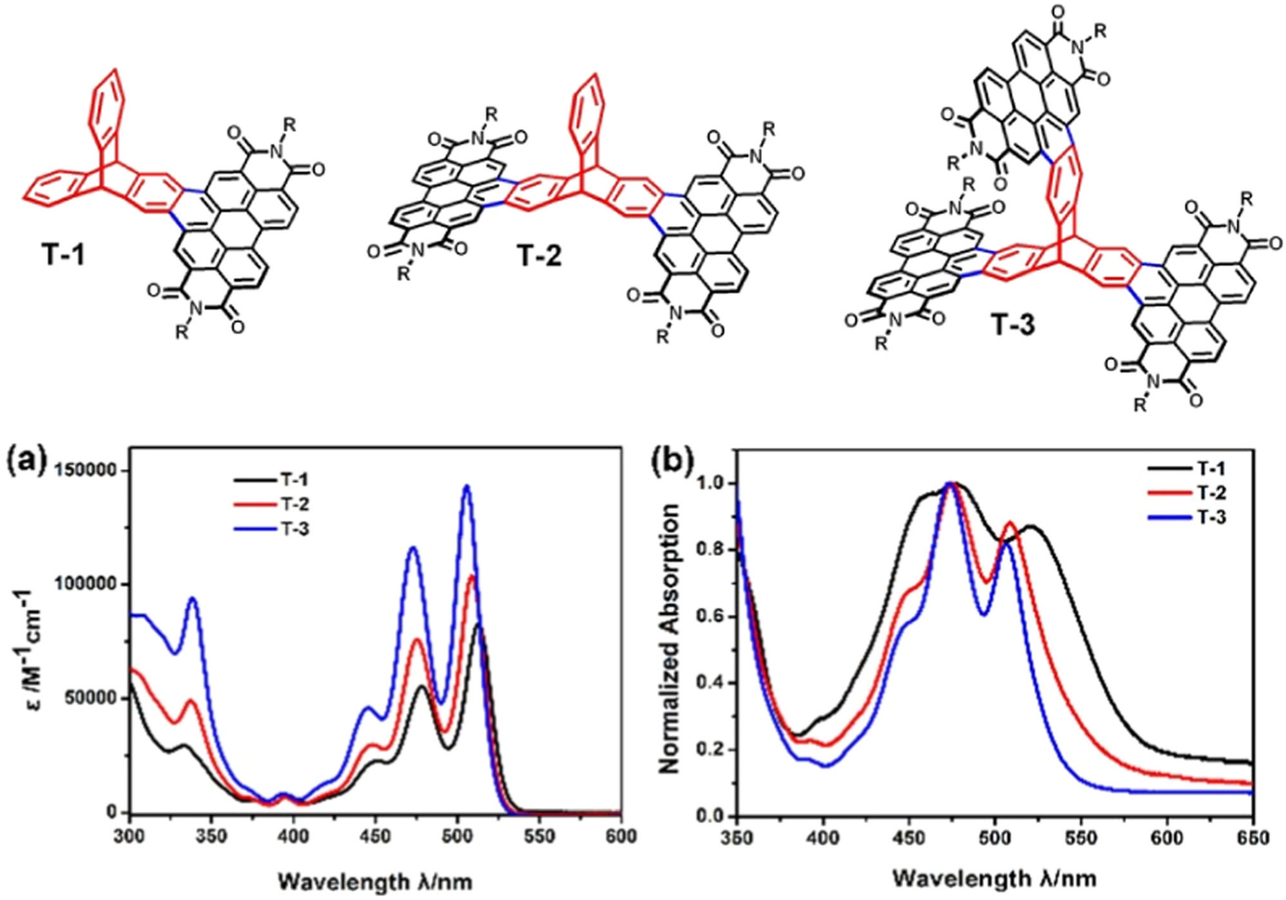

Fig. 15 Molecular structures of **PDI**-fused triptycene **T1–T3** (R = 6-undecyl) and their (a) $CHCl_3$ solution absorbance spectra and (b) thin film absorbance spectra. Adapted with permission from ref. 73. Copyright 2017, Wiley-VCH.

in Fig. 15). The overall waveform is sharp and structured, very like **TP3** and **PDI** itself. Compared to **TP3**, annulation of the PDI onto the triptycene core blueshifts the longest energy absorbance and the authors note a slight blueshift in the $\lambda_{\max}$ and widening of the optical E_g as more **PDI**-fused fins are appended. This was attributed to weakening of the molecular dipole upon addition of further electron accepting fins.

Across this series, no super-summative enhancements are observed. The ε of **T-1** is comparable to that of **PDI** itself (and by proxy **TP3**) and that of **T-2** is only slightly larger. **T-3** displays an ε which is approximately double that of **T-1**. DFT results for **T-3** show the HOMO is distributed over the entire molecule while the LUMO is spread uniformly over two of the **PDI** fins with minimal LUMO density over the triptycene. This is identical to the LUMO distribution of **T-2**. The frontier orbital layout for **T-1** is all positioned over the **PDI** fin. Cyclic voltammetry confirmed that the electron accepting strength of the molecules is essentially constant across the series, which indicates that the LUMO energy has not changed as fins have been added. Oxidation processes were not observed.

In terms of device performance for this series, **T-2** gave the best BHJ devices using **PTB7-Th** as a donor. **T-2** displayed PCE of 6.15% compared to 2.28% for **T-1** and 5.13% for **T-3** which had comparable J_{sc} but slightly lower FF. V_{oc} decreased gradually across the series as may be predicted from the blueshift in the UV spectra. **T-2** and **T-3** had a better balance of electron and hole mobilities which correlated with AFM results that indicated better film morphology for the **T-2** and **T-3** molecules.

A 2018 report by Kang *et al.* concerned triptycene **3**, (Fig. 16a) which was shown to undergo photoinduced hole transfer with single-walled carbon nanotubes.[74] The synthesis and properties of this compound alongside its first (**T-3**) and third (**4**) generation analogues followed in a subsequent contribution. Note that the smallest of these triptycenes **T-3** had also been presented in ref. 73. The results concerning **T-3** from these independent studies agree very well.

The helical **PDI** trimer **hPDI3** and a benzene-fused analogue **b-hPDI3** thereof (Fig. 16b) were employed as model compounds for comparison with **4**.[75] **hPDI3** had previously been studied by the same group in 2014 as one of a family of fused PDI oligomers alongside the dimer **hPDI2** and tetramer **hPDI4**.[76] These are helpful to consider when trying to understand the behaviour of **3** and **4**.

By DFT, **hPDI2–4** were shown to be non-planar due to steric repulsion between the C–H bonds of the cove regions of the **PDI** moieties. This results in helical or waggling geometries, or a mixture of the two in the case of **hPDI4**. The optimised

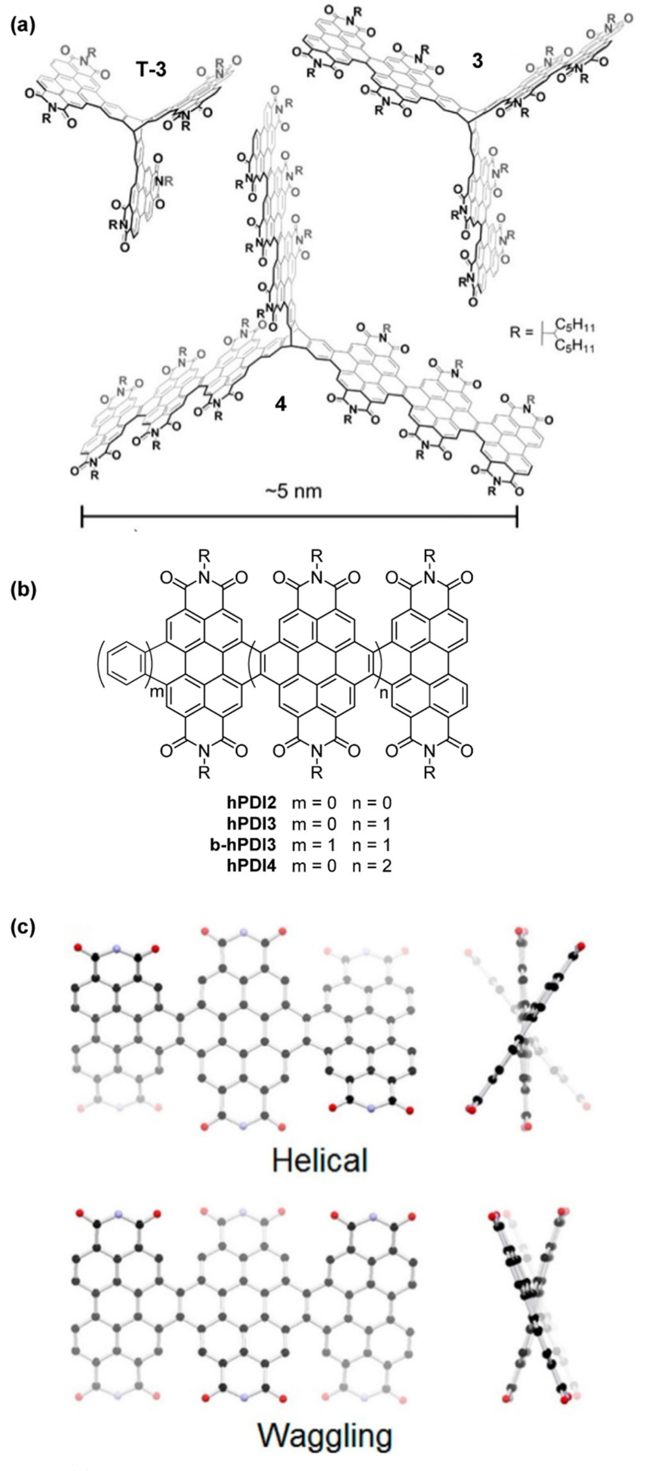

Fig. 16 (a) Molecular structures of fin-extended **PDI**-fused triptycenes **T-3**, **3** and **4**, Adapted with permission from ref. 75. Copyright 2018, American Chemical Society (b) the single-fin analogues **hPDI2–4** and benzo-fused single fin analogue **b-hPDI3**; (c) DFT optimised Helical and Waggling geometries for **hPDI3**. Reproduced with permission from ref. 76. Copyright 2014, American Chemical Society.

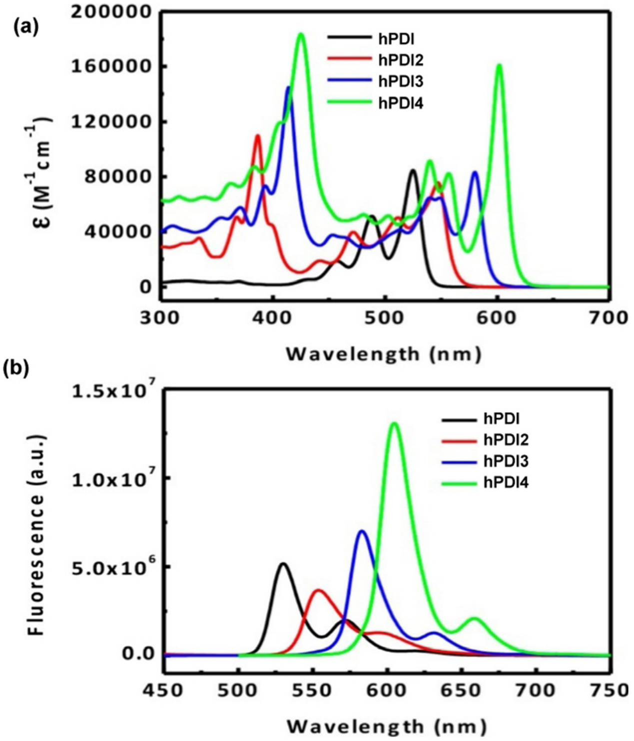

Fig. 17 (a) UV/vis absorbance spectra for **hPDI** (*N*,*N*′-bis(6-undecyl)**PDI**) and **hPDI2–4** in CH_2Cl_2 solution; (b) fluorescence spectra for **hPDI** and **hPDI2–4**. In CH_2Cl_2 solution. Reproduced with permission from ref. 76. Copyright 2014, American Chemical Society.

geometries of **hPDI3** are shown in Fig. 16c. The UV/vis and emission spectra for **hPDI2–4** (Fig. 17) display a red-shift as the oligomer length increases. The lowest energy absorbance is assigned to a simple HOMO-to-LUMO transition over the **PDI** chromophores. ε of this band is essentially constant between **PDI**, **hPDI2** and **hPDI3** but then increases dramatically by ∼100% for **hPDI4.** This enhancement is attributed to red-shifting of the symmetry-allowed transitions which are taking place from the HOMO−2 (over the carbon–carbon double bonds which fuse the **PDI** moieties together) into the LUMO. This red-shifting results in overlap with the HOMO-to-LUMO transition leading to the large increase in absorption intensity.

In the UV/vis spectra of the triptycenes **T-3, 3** and **4** (Fig. 18a) a similar sequential red-shift is observed for the lowest energy absorbance band with increasing fin length. An extremely high extinction coefficient ($\varepsilon > 600\,000\ \mathrm{M^{-1}\ cm^{-1}}$) is observed for the largest derivative **4.** This is over a 5-fold increase in ε compared to **hPDI3.** While benzene-fused **b-hPDI3** also displayed a higher ε than **hPDI3,** the homoconjugated triptycene still displays an increase in ε of over 35% compared to three times that of **b-hPDI3** (Fig. 18b).

While the DFT of **T-3, 3** and **4** indicated that the HOMO and LUMO have no presence over the central triptycene, with the frontier orbitals localised over the fins in a similar arrangement to **hPDI2–4,** TDDFT results showed that a manifold of low-lying excited states is present for **3** and **4.** It is difficult to conclude whether these arise from the complex symmetry adopted by the fins themselves, homoconjugation facilitated by the central triptycene or some combination of the two. It is clear that the influence of the extended three-dimensional structure is

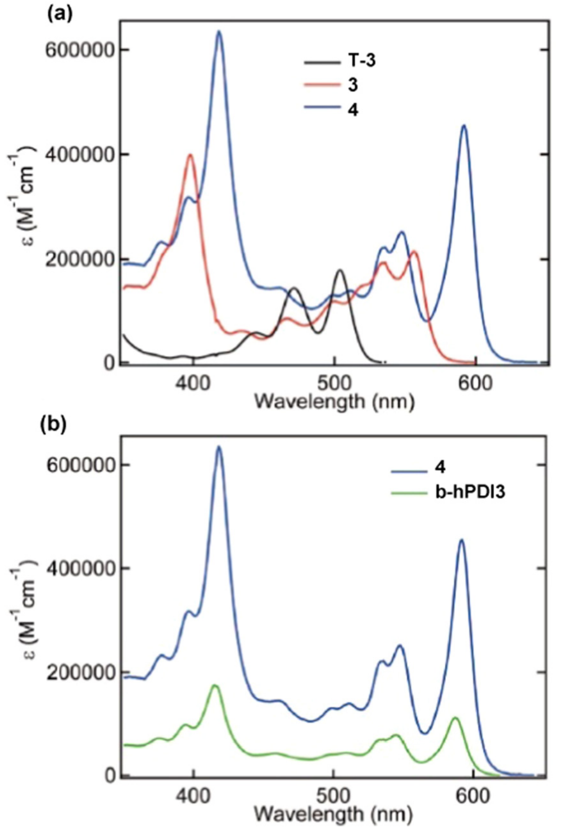

Fig. 18 UV/vis absorbance spectra for (a) **T-3**, **3** and **4** and (b) **4** and **b-hPDI3** in tetrahydrofuran solution. Adapted with permission from ref. 75. Copyright 2018, American Chemical Society.

distinct from simple ring fusion but the precise origins of super-summative enhancements in ε are challenging to pin down in these very large molecules.

Electrochemistry indicated that the oligo**PDI** fins were not electronically coupled. The cyclic voltammetry results revealed that each fin can be reduced simultaneously and in a stepwise fashion with each **PDI** moiety accepting two electrons. Therefore the largest molecule **4** is a reversible 18-e$^-$ acceptor. This is directly analogous to the multi-electron redox behaviour observed for the reduction of **TP3**, **SBF-PDI4**, and the oxidation of **3CzQ**. Electron paramagnetic resonance studies of **T-3** indicated that its radical anion is delocalised across all three fins which the authors attribute as being facilitated by transannular interactions over the homoconjugated triptycene core.

Triptycenes **3** and **4** were incorporated as electron transport materials in perovskite solar cells. Both outperformed PC$_{61}$BM with maximum efficiencies of 16.4% and 18% respectively. Combined with the results of SCLC measurements, the authors postulate that the longer fins penetrate more effectively into the perovskite layer thereby reducing contact resistance and improving overall device performance. The use of iptycenes as interface agents to modify film surfaces is reminiscent of the use of iptycenes to exert internal control over polymer morphology. This may represent a better use for triptycene derivatives in OSCs than as bulk active components themselves.

Though not studied for any specific application, a separate series of conceptually related, laterally-expanded electron-deficient ring-fused triptycenes **P1–P4** were published by Hu *et al.* in 2019.[77] In these examples the fins are composed of pyrene N-heteroacenes with diameters of up to 10.88 nm (Fig. 19) and show similarly complex variations in optical properties as the fin length increases.

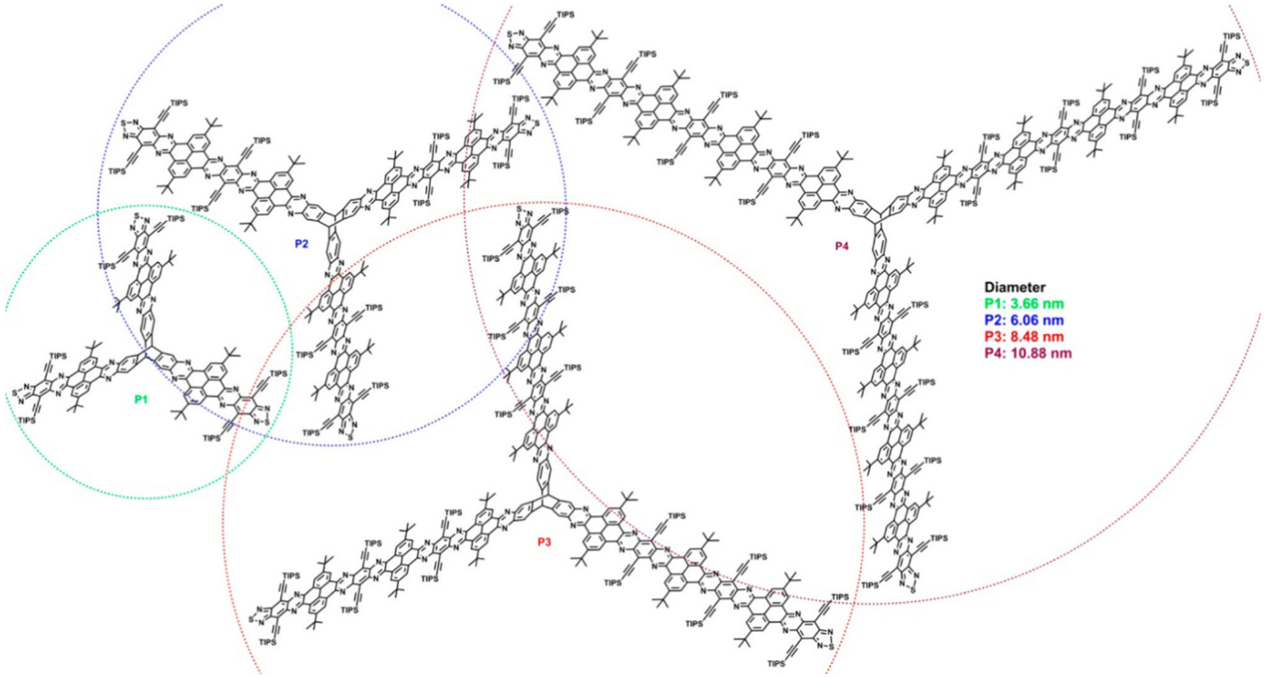

Fig. 19 Molecular structures of nanoscale extended triptycenes **P1–P4**. (Reproduced with permission from ref. 77. Copyright 2019, American Chemical Society.)

The pyrene units served to disrupt conjugation along the length of the fins therefore minimal redshift with increasing conjugation length was observed due to a gradual drop in LUMO energy as determined by cyclic voltammetry and DFT.

A theoretical study from 2019 by Sun *et al.* of 3D *vs.* 2D HTMs indicates that 3D structures have improved electron–hole dissociation characteristics which may help to improve performance, so pursuing large molecules such as **4** and **P4** as charge transport materials presents an important area for further development.[78]

Homoconjugated charge transport and energy storage materials

In 2018, Kwon *et al.* disclosed the triptycene hexaketone **TT** and diketone **TM** (structures in Fig. 20) and studied **TM** for energy storage applications.[79] Homoconjugation in the LUMO manifold was revealed from DFT analysis and cyclic voltammetry. Differential pulse voltammetry (DPV) revealed that **TT** could be reduced in single electron steps to the pentaanion (Fig. 20) with instabilities for the fully reduced hexaanion predicted using computational methods.

In a Li-ion half-cell, **TT** displayed an initial discharge capacity of 387 mA h g^{-1}. This approximated to 5.0 Li^{+} per molecule in agreement with the DPV results, although capacity had reduced by 55% after 20 charge/discharge cycles. Cycling performance could be enhanced in nanocomposite materials alongside the mesoporous carbon matrix CMK3.

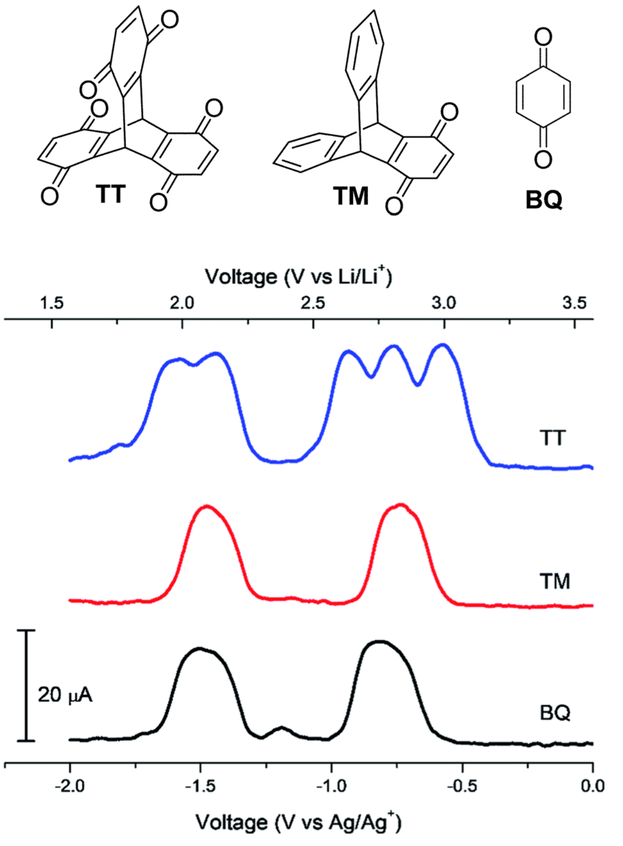

Fig. 20 Molecular structures of **TT**, **TM** and **BQ** and their DPV responses. Reproduced from ref. 79 with permission from the Royal Society of Chemistry.

Later in 2018 the Wuest group reported the isomeric triptycene hexaketone **8** which was synthesised by oxidation of 2,3,6,7,14,15-hexahydroxytriptycene **9**.[80] Transannular electronic effects meant that simple choice of oxidising agent permitted selective access to the partially oxidised 2,3-dione **10** and 2,3,6,7-tetraone **11** in good yields (structures in Fig. 21). The electrochemistry of **8** revealed that it could undergo reversible electrochemical reduction to a trianion in a step-wise fashion (Fig. 21a and b). It is worth highlighting the complementarity between the electrochemistry of the two electron poor tris(quinones) **TT** and **8** and the analogous hexa-alkoxytriptycenes studied by Rathore which were shown in Fig. 2.

Redox behaviour was apparent in the solid, crystalline state of dione **10** which was revealed to undergo reduction back to hexahydroxy **9** in a reversible topotactic reaction (Fig. 22). The presence of hydrazine vapours resulted in crystals of **10** changing from dark purple to colourless, this could then be reversed by exposure to HNO_3 vapours. As the molecules can undergo reversible redox reactions in the solid crystalline state these molecules provide some direction towards realising rechargeable carbon-based batteries.

[3.3.3]Propellanes – an alternative D_{3h} homoconjugated hydrocarbon

Finally, comparison with [3.3.3]propellanes, another class of three-finned hydrocarbon, gives some indication of how general the benefits of exploiting homoconjugation might be.

In two reports authored by Lv *et al.*[81,82] *peri*-extension of the peripheral naphthalene units of [3,3,3]propellane **12** formed perylene monoimide (**PMI**) moieties on one or more fins of the propellane core. The first paper concerned tris(**PMI**)propellane **13** (R = 6-undecyl) and bay-annulated derivatives **14–16** in a comparative study (structures shown in Fig. 23). Frontier orbitals were distributed across the entire surface of the molecule which led to multiple clearly separated peaks in cyclic voltammetry studies. *N*-6-Undecyl(**PMI**) itself was also studied as a single-fin analogue for comparison and was shown to have a maximum $\varepsilon = 33 \times 10^3$ M^{-1} cm^{-1}. Each of the propellanes **13–16** displayed a greater than four-fold enhancement of ε (Table 3) in comparison with the single-fin, with benzo-fused compound **14** displaying the largest $\varepsilon = 163 \times 10^3$ M^{-1} cm^{-1}. Single-crystal charge-carrier mobilities in the order of 10^{-3} cm^2 V^{-1} s^{-1} were obtained for **14** with the limited intermolecular overlap of the molecules observed in the crystal structure seeming to be a limiting factor in obtaining higher mobilities.

In the second of these reports, one- (**P-1**), two- (**P-2**), and three-finned (**P-3**) analogues of **13** featuring a larger alkyl group (R = 2-decyltetradecyl) were also produced (Fig. 24). **P-1** demonstrated very similar properties to *N*-2-decyltetradecyl(**PMI**) with only slightly red-shifted optical properties due to a narrower E_g.

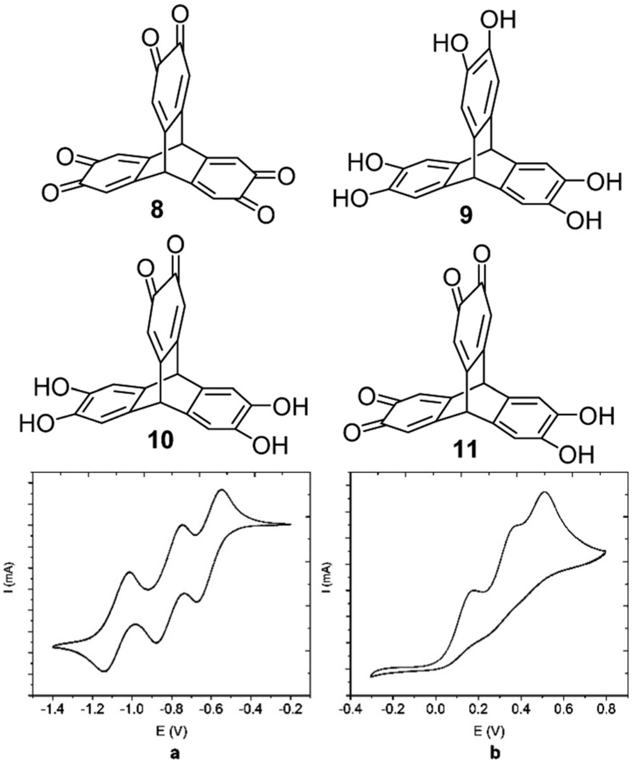

Fig. 21 Molecular structures of **8–10** and the cyclic voltammograms of (a) trisquinone **8** and (b) hexahydroxy **9**. Reproduced from ref. 80. Copyright 2018, American Chemical Society.

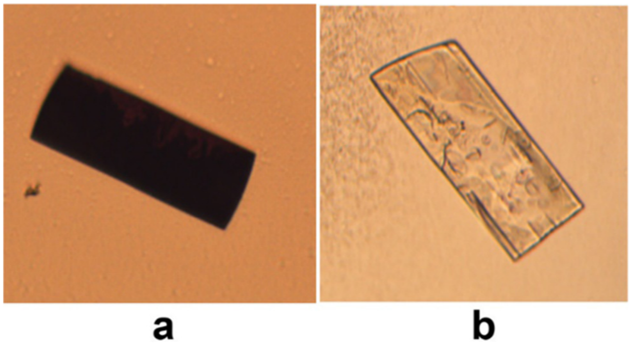

Fig. 22 Crystals of quinone **10** (a) before and (b) after exposure to N_2H_4 vapours. Reproduced from ref. 80. Copyright 2018, American Chemical Society.

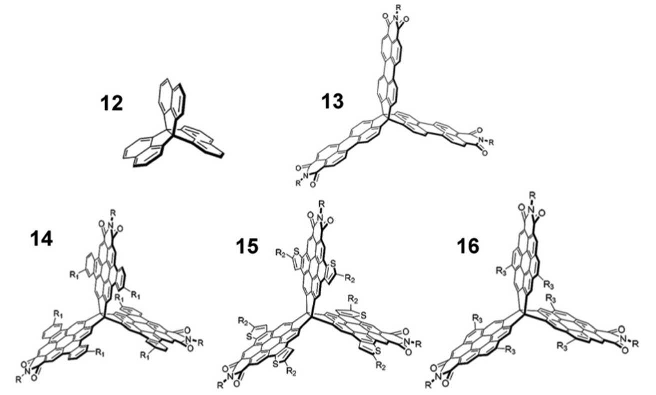

Fig. 23 Molecular structures of propellanes **12–16** R = 6-undecyl. Reproduced from ref. 81 with permission from the Royal Society of Chemistry.

Table 3 Summary of longest wavelength absorbance and emission characteristics for [3,3,3]propellanes **13–16** and **P-1**, **P-2** and **P-3**

	λ_{abs} (nm) [$\varepsilon \times 10^3$ M^{-1} cm^{-1}]	$\lambda_{\text{max PL}}$ (nm)	PLQY (%)
13	554 (152)	588	85
14	492 (163)	514	89
15	486 (137)	505	22
16	432 (122)	481	32
P-1	538 (35)	579	83
P-2	555 (81)	585	89
P-3	555 (152)	588	85

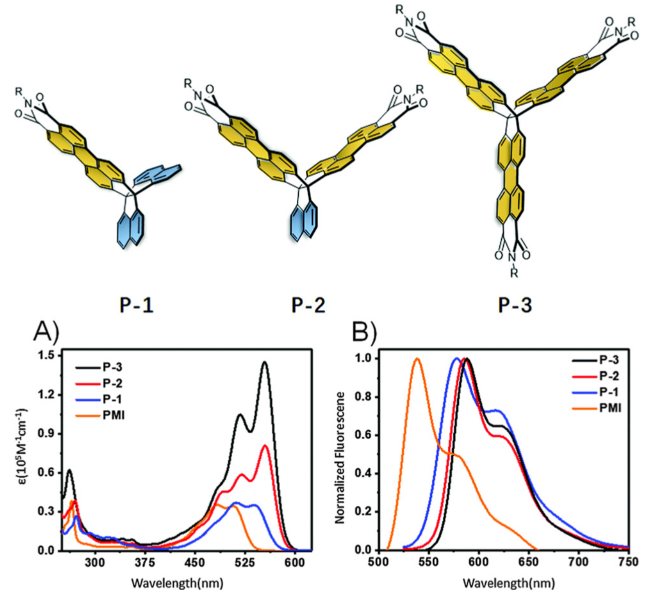

Fig. 24 Molecular structures of **P-1**, **P-2** and **P-3**, and their (A) absorbance spectra and, (B) photoluminescence spectra. Reproduced from ref. 82 with permission from the Chinese Chemical Society (CCS), Institute of Chemistry of Chinese Academy of Sciences (IC), and the Royal Society of Chemistry.

The influence of homoconjugation becomes apparent in the absorbance spectra of these compounds (Fig. 24A) with the ε of **P-2** (81 × 10^3 M^{-1} cm^{-1}) being slightly more than double that of both **P-1** 35 × 10^3 M^{-1} cm^{-1}) and *N*-2-decyltetradecyl(**PMI**) (34 × 10^3 M^{-1} cm^{-1}) while the molar absorptivity almost doubles again for **P-3** (ε = 152 × 10^3 M^{-1} cm^{-1}). The fluorescence quantum yields displayed very little variation across the series staying well over 80% in all cases.

OFET devices were produced and demonstrated mobilities of 2.2 × 10^{-4} cm^2 V^{-1} s^{-1} and 3.5 × 10^{-4} cm^2 V^{-1} s^{-1} for **P-1** and **P-2** respectively, while **P-3** was an entire order of magnitude lower at 2.5 × 10^{-5} cm^2 V^{-1} s^{-1} which was ascribed to limited crystallinity in the film. **P-1** and **P-2** also displayed better performance in OLED devices in all parameters.

Outlook

The preceding sections highlight numerous positive effects that can be observed by exploiting homoconjugation in triptycene chromophores/electrophores. The primary benefits are:

(1) Amplified molar absorptivity.

(2) Accelerated radiative decay.

(3) Generation of multiple charge carriers over small potential windows.

Considering the first two points design rules to obtain hyperchromic, potentially super-summative, enhancements in ε, and f_{osc} can be proposed. Firstly, ensuring that the LUMO is localised on the homoconjugated core of the triptycene and straddles two or more of the fins appears to be essential. This gives rise to a manifold of low-lying excited states which interact constructively to facilitate the observed enhancements. Secondly, molecules featuring ring-fused structures and/or some dipole moment on the fins of the molecule tend to show greater enhancements than structures without an obvious dipole moment. This is intuitive and seemingly general until much longer extended chromophore fins are present.

The third benefit concerning electrochemical properties is realised in molecular designs which use electron donating or withdrawing substituents to modulate the frontier orbital density over the centre of the triptycene core. A lower amount of MO density at the homoconjugated core will lead to more redox events occuring over a smaller potential window and *vice versa* for molecules with large amounts of MO density over the triptycene core. Choice of substituent and regiochemistry permits control over both the magnitude of the potential window that the charges are generated over, and the nature of the charge carriers themselves.

However, challenges associated with using triptycenes also present themselves. These are usually associated with the morphology of neat films of triptycenes being poor due to the IFV of the molecules inhibiting tight packing. While this can have negative impacts on the performance of devices based upon concentrated thin films of these molecules such as BHJ OSCs or OFET devices, it is important to highlight that poor morphology is certainly not a general property of triptycenes when engineered properly. An important series of triptycenes with *peri*-alkoxy substituents demonstrated exceptionally good self-assembly properties which evidences this well.[27,83,84]

Bearing these points in mind, we can start to speculate on how to further harness the benefits of homoconjugation effects for the applications discussed.

OLED and luminescent materials

The performance of luminophores based on D–A architectures, particularly TADF emitters, can benefit greatly from the combination of very high ε and f_{osc} which occur in the ICT bands of D–A triptycenes. This provides a realistic route to improve the effectiveness of red luminophores in particular, the efficiencies of which suffer due to the energy gap law which leads to rapid thermal NRD outcompeting radiative decay.[85,86]

As it is the LUMO which must display homoconjugation to achieve enhancements structural modifications of the triptycene core itself will be required to further develop this concept. This could be achieved by using a wider variety of N-heterocyclic triptycenes or appending peripheral electron-withdrawing substituents onto the triptycene prior to addition of the donor moieties. In all other respects standard TADF design rules can be employed to control the emission wavelength.[87–89]

Morphological concerns are mitigated against in a typical doped OLED architecture as the luminophores are distributed in a small quantity throughout a bulk host matrix. As such, the main challenges presented in this context are ultimately the same as for TADF emitters in general. FWHM are too large leading to poor colour purity, however the use of multi-resonant TADF design principles may provide a route to circumventing this.[90–92]

OSC materials

Maximising the light absorbance across the optical band gap is one approach to obtaining higher PCEs. A higher ε results in improved absorbance of sunlight and diminished NRD thereby enhancing the V_{OC} of a device, so hyperchromic enhancements in ε should produce better devices overall. This will be particularly important for sensitisers which have a suboptimal overlap with the solar spectrum.[93–95]

Considering the very high ε that have been obtained in appropriately designed triptycenes such as **3Cbz**, **C_{3V}-E/B-TTAI**, **C_S-E/B-TTAI**, **3** and **4**, homoconjugation emerges as appealing avenue to explore for high ε materials which can be used a variety of OSC architectures. To date, studies of BHJ OSC devices using triptycene NFAs have demonstrated relatively poor performance. This is due to a combination of the structures studied to date not adhering to the LUMO-core, HOMO-shell motif required for major enhancements in ε, alongside poor BHJ morphology. The previously mentioned self-organised films of *peri*-alkoxy substituted triptycenes and the use of triptycene itself as a dopant to improve morphology and efficiencies in BHJ OSCs[24] and other devices[83,96–98] indicate that careful consideration of substitution patterns or device processing and manufacture might be used to overcome film morphology challenges.

We highlight that other photovoltaic device architectures such as dye-sensitised (DSSC) and perovskite solar cells (PSCs) may present greater opportunities for exploiting homoconjugation as well as circumventing the morphology problems encountered in BHJ devices. In PSCs **4** was used as a interfacing agent between the electron transport and perovskite layers rather than a bulk component. This produced devices with efficiency up to 18% which further demonstrates the power of triptycenes as additives. In DSSCs existing triptycene containing dyes only use triptycene as a bulky substituent rather than as a functional part of the chromophore or anchoring moeity.[99,100] Triptycenes can show very strong bi-/tripodal anchoring to surfaces[96,101,102] and homoconjugation can provide the high ε and tunable E_g required for harvesting solar energy. New materials designed according to the general rules proposed at the start of this Outlook section and incorporating suitable anchoring groups could thereby produce excellent new dyes for DSSCs.

Charge transport and energy storage materials

The electrochemical implications of a homoconjugated HOMO were demonstrated well by the alkoxy bearing molecules **T23** and **T14** which showed that by decreasing the extent of transannular orbital overlap the potential window required to assume a stable tricationic state decreased concomitantly by $\sim$500 mV and was obtained after just -1.2 V *vs.* Fc/Fc$^+$. The LUMO can be manipulated in the same fashion to produce n-type systems. For example, **3Pxz** had a homoconjugated LUMO which allowed a reversible three step reduction to take place at +0.73 V *vs.* Fc/Fc$^+$ while **4** could be reversibly reduced to a remarkable octadecyl anion over a potential window of less than 1.5 V. Similar reductive behaviour was observed in quinones **TT** and **8**. Furthermore, the triptycene core can be used indirectly to isolate the HOMO or LUMO on the periphery of a molecule leading to single-step generation of multiple charge carriers simultaneously as shown in **3Cbz** and **hPDI2–4**.

At first glance, the ability to easily generate many charge carriers from an individual organic molecule could foreseeably realise higher charge carrier density and ON/OFF ratios in charge transport devices such as OFETs. However, we would argue that what really sets the electrochemical properties of triptycenes apart is the stability of the multiply-charged states obtained. Generating very highly charged states typically causes major electrochemical stress in organic molecules but the homoconjugated materials presented to date are very robust. Building from this, triptycene-based compounds present valid alternatives to the anthraquinone systems which are under the most intense development.[103] In this fashion they provide scope for use not only in traditional alkali metal systems but also for more exotic or highly charge ions such as Al^{3+}.[104,105] The 3D structure of triptycenes is well suited for incorporation into porous COF or MOF architectures which probably present the best route for further development in this context.

Conclusions

This review has aimed to provide initial insights towards harnessing homoconjugation in triptycene based molecular materials and what might be achieved by doing so.

This effect can clearly be used to induce very high magnitude enhancements in useful optoelectronic properties, however there is often a trade-off between obtaining the maximum enhancement in properties and the performance of thin films of said molecules in devices. This is most notable for triptycenes in which all three fins have been functionalised. These tend to display both the biggest enhancements in properties but also the lowest quality films in devices. As such, triptycenes which display properties influenced by homoconjugation have not yet translated to notably high performance in neat or very concentrated thin film devices such as OFETs or BHJ OSCs but when used as dilute dopants in OLEDs or perovskite OSCs the three-finned triptycenes perform much better. This observation must be considered in the design and study of future homoconjugated chromophores and electrophores to obtain improved device performance. We note that few studies have deliberately set out to actively use homoconjugation, therefore a more considered approach to molecular design will lead rapidly to improved device performance from this class of materials and we have proposed some design rules towards this end.

Finally, while this review has focussed largely upon triptycenes, numerous other homoconjugated scaffolds are available. These include the spirobifluorenes and propellanes, which have been mentioned here, alongside less rigid chemical fragments such as diphenylmethanes and bisphenols. As such, there is great scope for more expansive utility of homoconjugation and the benefits it can bring in controlling functional molecular properties.

Conflicts of interest

There are no conflicts of interest to declare.

Acknowledgements

J.-R. M. thanks the EPSRC Sustainable Hydrogen CDT (EP/S023909) and Loughborough University for support. S. M. thanks Loughborough University for a PhD studentship. I. A. W. thanks the EPSRC for support (EP/T028688/1 and EP/V048554/1).

Notes and references

1 D. K. Frantz, A. Linden, K. K. Baldridge and J. S. Siegel, *J. Am. Chem. Soc.*, 2012, **134**, 1528–1535.

2 S. Toyota, K. Kawahata, K. Sugahara, K. Wakamatsu and T. Iwanaga, *Eur. J. Org. Chem.*, 2017, 5696–5707.

3 T. R. Kelly, *Acc. Chem. Res.*, 2001, **34**, 514–522.

4 T. R. Kelly, H. De Silva and R. A. Silva, *Nature*, 1999, **401**, 150–152.

5 C. Joachim, H. Tang, F. Moresco, G. Rapenne and G. Meyer, *Nanotechnology*, 2002, **13**, 330–335.

6 T. Nishino, C. J. Martin, H. Takeuchi, F. Lim, K. Yasuhara, Y. Gisbert, S. Abid, N. Saffon-Merceron, C. Kammerer and G. Rapenne, *Chem. – Eur. J.*, 2020, **26**, 11913.

7 F. Bertani, N. Riboni, F. Bianchi, G. Brancatelli, E. S. Sterner, R. Pinalli, S. Geremia, T. M. Swager and E. Dalcanale, *Chem. – Eur. J.*, 2016, **22**, 3312–3319.

8 S. Barman, J. A. Garg, O. Blacque, K. Venkatesan and H. Berke, *Chem. Commun.*, 2012, **48**, 11127–11129.

9 A. Fuoco, B. Comesana-Gandara, M. Longo, E. Esposito, M. Monteleone, I. Rose, C. G. Bezzu, M. Carta, N. B.

McKeown and J. C. Jansen, *ACS Appl. Mater. Interfaces*, 2018, **10**, 36475–36482.

10 M. Lee, C. G. Bezzu, M. Carta, P. Bernardo, G. Clarizia, J. C. Jansen and N. B. McKeown, *Macromolecules*, 2016, **49**, 4147–4154.

11 X. H. Ma, Z. Y. Zhu, W. X. Shi, W. H. Ji, J. X. Li, Y. G. Wang and I. Pinnau, *J. Mater. Chem. A*, 2021, **9**, 5404–5414.

12 Q. Liang, J. Liu, Y. Wei, Z. Zhao and M. J. MacLachlan, *Chem. Commun.*, 2013, **49**, 8928–8930.

13 K. Preet, G. Gupta, M. Kota, S. K. Kansal, D. B. Salunke, H. K. Sharma, S. C. Sahoo, P. Van der Voort and S. Roy, *Cryst. Growth Des.*, 2019, **19**, 2525–2530.

14 Q. Liang, G. Y. Jiang, Z. Zhao, Z. Y. Li and M. J. MacLachlan, *Catal. Sci. Technol.*, 2015, **5**, 3368–3374.

15 A. M. Elewa, M. H. Elsayed, A. F. M. El-Mahdy, C. L. Chang, L. Y. Ting, W. C. Lin, C. Y. Lu and H. H. Chou, *Appl. Catal., B*, 2021, **285**, 119802.

16 T. Ikai, T. Yoshida, S. Awata, Y. Wada, K. Maeda, M. Mizuno and T. M. Swager, *ACS Macro Lett.*, 2018, **7**, 364–369.

17 T. Ikai, T. Yoshida, K. I. Shinohara, T. Taniguchi, Y. Wada and T. M. Swager, *J. Am. Chem. Soc.*, 2019, **141**, 4696–4703.

18 Z. Chen, P. Li, R. Anderson, X. Wang, X. Zhang, L. Robison, L. R. Redfern, S. Moribe, T. Islamoglu, D. A. Gomez-Gualdron, T. Yildirim, J. F. Stoddart and O. K. Farha, *Science*, 2020, **368**, 297–303.

19 Z. Chen, P. Li, X. Zhang, M. R. Mian, X. Wang, P. Li, Z. Liu, M. O'Keeffe, J. F. Stoddart and O. K. Farha, *Nano Res.*, 2021, **14**, 376–380.

20 Y. Wang, C. Wu, W. Sun, Q. Pan, W. Hao, H. Liu, J. Sun, Z. Li, J. Sun and Y. Zhao, *Mater. Chem. Front.*, 2021, **5**, 944–949.

21 N. Baig, S. Shetty, S. Al-Mousawi, F. Al-Sagheer and B. Alameddine, *React. Funct. Polym.*, 2019, **139**, 153–161.

22 A. Lohr and T. M. Swager, *J. Mater. Chem.*, 2010, **20**, 8107–8111.

23 Z. Chen and T. M. Swager, *Macromolecules*, 2008, **41**, 6880–6885.

24 L. Krishnan Jagadamma, L. J. McCarron, A. A. Wiles, V. Savikhin, M. T. Sajjad, M. Yazdani, V. M. Rotello, M. F. Toney, G. Cooke and I. D. W. Samuel, *ACS Appl. Mater. Interfaces*, 2018, **10**, 24665–24678.

25 R. G. Taylor, C. G. Bezzu, M. Carta, K. J. Msayib, J. Walker, R. Short, B. M. Kariuki and N. B. McKeown, *Chem. – Eur. J.*, 2016, **22**, 2466–2472.

26 R. G. Taylor, M. Carta, C. G. Bezzu, J. Walker, K. J. Msayib, B. M. Kariuki and N. B. McKeown, *Org. Lett.*, 2014, **16**, 1848–1851.

27 N. Seiki, Y. Shoji, T. Kajitani, F. Ishiwari, A. Kosaka, T. Hikima, M. Takata, T. Someya and T. Fukushima, *Science*, 2015, **348**, 1122–1126.

28 (*a*) See: **https://goldbook.iupac.org/terms/view/H02842**; (*b*) P. Muller, *Pure Appl. Chem.*, 1994, **66**, 1077–1184.

29 R. V. Williams, *Chem. Rev.*, 2001, **101**, 1185–1204.

30 P. D. Bartlett, M. J. Ryan and S. G. Cohen, *J. Am. Chem. Soc.*, 1942, **64**, 2649–2653.

31 P. D. Bartlett and E. S. Lewis, *J. Am. Chem. Soc.*, 1950, **72**, 1005–1009.

32 J. Hine, J. A. Brown, L. H. Zalkow, W. E. Gardner and M. Hine, *J. Am. Chem. Soc.*, 1955, **77**, 594–598.

33 H. E. Zimmerman and R. M. Paufler, *J. Am. Chem. Soc.*, 1960, **82**, 1514–1515.

34 C. F. Wilcox, Jr., S. Winstein and W. G. McMillan, *J. Am. Chem. Soc.*, 1960, **82**, 5450–5454.

35 P. Bischof, J. A. Hashmall, E. Heilbronner and V. Hornung, *Helv. Chim. Acta*, 1969, **52**, 1745–1749.

36 E. Haselbach, E. Heilbronner and G. Schröder, *Helv. Chim. Acta*, 1971, **54**, 153–162.

37 R. Hoffmann, E. Heilbronner and R. Gleiter, *J. Am. Chem. Soc.*, 1970, **92**, 706–707.

38 T. Nakazawa and I. Murata, *J. Am. Chem. Soc.*, 1977, **99**, 1996–1997.

39 H.-D. Martin, B. Mayer, R. Gleiter, W. Schäfer and F. Vögtle, *Chem. Ber.*, 1983, **116**, 2546–2553.

40 H.-D. Martin and B. Mayer, *Angew. Chem., Int. Ed. Engl.*, 1983, **22**, 283–314.

41 K. Baumgartner, M. Hoffmann, F. Rominger, S. M. Elbert, A. Dreuw and M. Mastalerz, *J. Org. Chem.*, 2020, **85**, 15256–15272.

42 S. M. Elbert, T. Kirschbaum, F. Rominger and M. Mastalerz, *Org. Mater.*, 2021, **03**, 097–102.

43 M. R. Talipov, T. S. Navale and R. Rathore, *Angew. Chem., Int. Ed.*, 2015, **54**, 14468–14472.

44 M. V. Ivanov, S. A. Reid and R. Rathore, *J. Phys. Chem. Lett.*, 2018, **9**, 3978–3986.

45 K. Kawasumi, T. Wu, T. Zhu, H. S. Chae, T. Van Voorhis, M. A. Baldo and T. M. Swager, *J. Am. Chem. Soc.*, 2015, **137**, 11908–11911.

46 F. B. Dias, T. J. Penfold and A. P. Monkman, *Methods Appl. Fluoresc.*, 2017, **5**, 012001.

47 P. Lei, S. Zhang, N. Zhang, X. Yin, N. Wang and P. Chen, *ACS Omega*, 2020, **5**, 28606–28614.

48 W. Huang, M. Einzinger, T. Zhu, H. S. Chae, S. Jeon, S.-G. Ihn, M. Sim, S. Kim, M. Su, G. Teverovskiy, T. Wu, T. Van Voorhis, T. M. Swager, M. A. Baldo and S. L. Buchwald, *Chem. Mater.*, 2018, **30**, 1462–1466.

49 R. Qian, H. Tong, C. Huang, J. Li, Y. Tang, R. Wang, K. Lou and W. Wang, *Org. Biomol. Chem.*, 2016, **14**, 5007–5011.

50 S. Montanaro, D. G. Congrave, M. K. Etherington and I. A. Wright, *J. Mater. Chem. C*, 2019, **7**, 12886–12890.

51 M. K. Etherington, J. Gibson, H. F. Higginbotham, T. J. Penfold and A. P. Monkman, *Nat. Commun.*, 2016, **7**, 13680.

52 L. S. Cui, A. J. Gillett, S. F. Zhang, H. Ye, Y. Liu, X. K. Chen, Z. S. Lin, E. W. Evans, W. K. Myers, T. K. Ronson, H. Nakanotani, S. Reineke, J. L. Bredas, C. Adachi and R. H. Friend, *Nat. Photonics*, 2020, **14**, 636–642.

53 H. Noda, X. K. Chen, H. Nakanotani, T. Hosokai, M. Miyajima, N. Notsuka, Y. Kashima, J. L. Bredas and C. Adachi, *Nat. Mater.*, 2019, **18**, 1084–1090.

54 S. Montanaro, P. Pander, J. R. Mistry, M. R. J. Elsegood, S. J. Teat, A. D. Bond, I. A. Wright, D. G. Congrave and M. K. Etherington, *J. Mater. Chem. C*, 2022, **10**, 6306–6313.

55 L. Yu, Z. Wu, C. Zhong, G. Xie, Z. Zhu, D. Ma and C. Yang, *Adv. Opt. Mater.*, 2017, **5**, 1700588.

56 T. Liu and A. Troisi, *Adv. Mater.*, 2013, **25**, 1038–1041.

57 Y. Yang, C. Yao, L. Li, M. Bo, J. Zhang, C. Peng and J. Wang, *RSC Adv.*, 2020, **10**, 12004–12012.

58 E. H. Menke, V. Lami, Y. Vaynzof and M. Mastalerz, *Chem. Commun.*, 2016, **52**, 1048–1051.

59 S. Maniam, H. F. Higginbotham, T. D. M. Bell and S. J. Langford, *Chem. – Eur. J.*, 2019, **25**, 7044–7057.

60 E. H. Menke, D. Leibold, V. Lami, Y. J. Hofstetter, M. Mastalerz and Y. Vaynzof, *Org. Electron.*, 2017, **47**, 211–219.

61 E. H. Menke, D. Leibold, A. P. Ullrich, Y. Vaynzof and M. Mastalerz, *Org. Chem. Front.*, 2017, **4**, 834–838.

62 E. H. Menke, D. Leibold, F. J. Berger, F. Rominger, Y. Vaynzof and M. Mastalerz, *ChemPlusChem*, 2017, **82**, 1390–1395.

63 C. Li and H. Wonneberger, *Adv. Mater.*, 2012, **24**, 613–636.

64 A. Nowak-Król and F. Würthner, *Org. Chem. Front.*, 2019, **6**, 1272–1318.

65 V. Sharma, J. D. B. Koenig and G. C. Welch, *J. Mater. Chem. A*, 2021, **9**, 6775–6789.

66 X. Liu, Y. Cai, X. Huang, R. Zhang and X. Sun, *J. Mater. Chem. C*, 2017, **5**, 3188–3194.

67 S. Chen, Y. Liu, W. Qiu, X. Sun, Y. Ma and D. Zhu, *Chem. Mater.*, 2005, **17**, 2208–2215.

68 A. J. Jimenez, F. Spanig, M. S. Rodriguez-Morgade, K. Ohkubo, S. Fukuzumi, D. M. Guldi and T. Torres, *Org. Lett.*, 2007, **9**, 2481–2484.

69 J. Yi, Y. Wang, Q. Luo, Y. Lin, H. Tan, H. Wang and C. Q. Ma, *Chem. Commun.*, 2016, **52**, 1649–1652.

70 T. P. Saragi, T. Spehr, A. Siebert, T. Fuhrmann-Lieker and J. Salbeck, *Chem. Rev.*, 2007, **107**, 1011–1065.

71 H. E. Simmons and T. Fukunaga, *J. Am. Chem. Soc.*, 1967, **89**, 5208–5215.

72 J. Lee, R. Singh, D. H. Sin, H. G. Kim, K. C. Song and K. Cho, *Adv. Mater.*, 2016, **28**, 69–76.

73 D. Meng, H. Fu, B. Fan, J. Zhang, Y. Li, Y. Sun and Z. Wang, *Chem. – Asian J.*, 2017, **12**, 1286–1290.

74 H. S. Kang, T. J. Sisto, S. Peurifoy, D. H. Arias, B. Y. Zhang, C. Nuckolls and J. L. Blackburn, *J. Phys. Chem. C*, 2018, **122**, 14150–14161.

75 S. R. Peurifoy, E. Castro, F. Liu, X. Y. Zhu, F. Ng, S. Jockusch, M. L. Steigerwald, L. Echegoyen, C. Nuckolls and T. J. Sisto, *J. Am. Chem. Soc.*, 2018, **140**, 9341–9345.

76 Y. Zhong, B. Kumar, S. Oh, M. T. Trinh, Y. Wu, K. Elbert, P. Li, X. Zhu, S. Xiao, F. Ng, M. L. Steigerwald and C. Nuckolls, *J. Am. Chem. Soc.*, 2014, **136**, 8122–8130.

77 B. L. Hu, C. An, M. Wagner, G. Ivanova, A. Ivanova and M. Baumgarten, *J. Am. Chem. Soc.*, 2019, **141**, 5130–5134.

78 Z. Z. Sun, S. Feng, C. Gu, N. Cheng and J. Liu, *Phys. Chem. Chem. Phys.*, 2019, **21**, 15206–15214.

79 J. E. Kwon, C. S. Hyun, Y. J. Ryu, J. Lee, D. J. Min, M. J. Park, B. K. An and S. Y. Park, *J. Mater. Chem. A*, 2018, **6**, 3134–3140.

80 S. Langis-Barsetti, T. Maris and J. D. Wuest, *J. Org. Chem.*, 2018, **83**, 15426–15437.

81 L. Lv, W. Sun, Z. Jia, G. Zhang, F. Wang, Z. Tan and L. Zhang, *Mater. Chem. Front.*, 2020, **4**, 3539–3545.

82 L. Lv, J. Roberts, C. Xiao, Z. Jia, W. Jiang, G. Zhang, C. Risko and L. Zhang, *Chem. Sci.*, 2019, **10**, 4951–4958.

83 T. Yokota, T. Kajitani, R. Shidachi, T. Tokuhara, M. Kaltenbrunner, Y. Shoji, F. Ishiwari, T. Sekitani, T. Fukushima and T. Someya, *Nat. Nanotechnol.*, 2018, **13**, 139–144.

84 T. Imaizumi, R. Takehara, Y. Yamashita, T. Yagi, F. Ishiwari, Y. Shoji, X. Wang, Y. Murakami, T. Nishino and T. Fukushima, *Jpn. J. Appl. Phys.*, 2021, **60**, 038002.

85 N. Notsuka, H. Nakanotani, H. Noda, K. Goushi and C. Adachi, *J. Phys. Chem. Lett.*, 2020, **11**, 562–566.

86 J. Eng and T. J. Penfold, *Chem. Rec.*, 2020, **20**, 831–856.

87 Y. Im, M. Kim, Y. J. Cho, J.-A. Seo, K. S. Yook and J. Y. Lee, *Chem. Mater.*, 2017, **29**, 1946–1963.

88 W. Che, Y. Xie and Z. Li, *Asian J. Org. Chem.*, 2020, **9**, 1262–1276.

89 P. de Silva, C. A. Kim, T. Zhu and T. Van Voorhis, *Chem. Mater.*, 2019, **31**, 6995–7006.

90 H. J. Kim and T. Yasuda, *Adv. Opt. Mater.*, 2022, **10**, 2201714.

91 S. Madayanad Suresh, D. Hall, D. Beljonne, Y. Olivier and E. Zysman-Colman, *Adv. Funct. Mater.*, 2020, **30**, 1908677.

92 G. Meng, L. Liu, Z. He, D. Hall, X. Wang, T. Peng, X. Yin, P. Chen, D. Beljonne, Y. Olivier, E. Zysman-Colman, N. Wang and S. Wang, *Chem. Sci.*, 2022, **13**, 1665–1674.

93 M. S. Vezie, S. Few, I. Meager, G. Pieridou, B. Dörling, R. S. Ashraf, A. R. Goñi, H. Bronstein, I. McCulloch, S. C. Hayes, M. Campoy-Quiles and J. Nelson, *Nat. Mater.*, 2016, **15**, 746–753.

94 J. Yan, X. Rodríguez-Martínez, D. Pearce, H. Douglas, D. Bili, M. Azzouzi, F. Eisner, A. Virbule, E. Rezasoltani, V. Belova, B. Dörling, S. Few, A. A. Szumska, X. Hou, G. Zhang, H.-L. Yip, M. Campoy-Quiles and J. Nelson, *Energy Environ. Sci.*, 2022, **15**, 2958–2973.

95 A. Markina, K.-H. Lin, W. Liu, C. Poelking, Y. Firdaus, D. R. Villalva, J. I. Khan, S. H. K. Paleti, G. T. Harrison, J. Gorenflot, W. Zhang, S. De Wolf, I. McCulloch, T. D. Anthopoulos, D. Baran, F. Laquai and D. Andrienko, *Adv. Energy Mater.*, 2021, **11**, 2102363.

96 S. Das, G. Nascimbeni, R. O. de la Morena, F. Ishiwari, Y. Shoji, T. Fukushima, M. Buck, E. Zojer and M. Zharnikov, *ACS Nano*, 2021, **15**, 11168–11179.

97 M. Sugiyama, S. Jancke, T. Uemura, M. Kondo, Y. Inoue, N. Namba, T. Araki, T. Fukushima and T. Sekitani, *Org. Electron.*, 2021, **96**, 106219.

98 F. K.-C. Leung, F. Ishiwari, T. Kajitani, Y. Shoji, T. Hikima, M. Takata, A. Saeki, S. Seki, Y. M. A. Yamada and T. Fukushima, *J. Am. Chem. Soc.*, 2016, **138**, 11727–11733.

99 M. Yan, Q.-H. Wang, Y.-Z. Zhu, M.-L. Han, Y.-Q. Yan and J.-Y. Zheng, *J. Photochem. Photobiol., A*, 2021, **416**, 113325.

100 M. Yan, Y.-Z. Zhu, Y.-Q. Yan, Q.-H. Wang, G.-L. Yin and J.-Y. Zheng, *J. Photochem. Photobiol., A*, 2022, **433**, 114132.

101 F. Ishiwari, G. Nascimbeni, E. Sauter, H. Tago, Y. Shoji, S. Fujii, M. Kiguchi, T. Tada, M. Zharnikov, E. Zojer and T. Fukushima, *J. Am. Chem. Soc.*, 2019, **141**, 5995–6005.

102 S. Das, A. Asyuda, Y. Shoji, A. Kosaka, T. Fukushima and M. Zharnikov, *J. Phys. Chem. C*, 2021, **125**, 18968–18978.

103 Y. Wu, R. Zeng, J. Nan, D. Shu, Y. Qiu and S.-L. Chou, *Adv. Energy Mater.*, 2017, **7**, 1700278.

104 S. K. Das, S. Mahapatra and H. Lahan, *J. Mater. Chem. A*, 2017, **5**, 6347–6367.

105 D. J. Kim, D.-J. Yoo, M. T. Otley, A. Prokofjevs, C. Pezzato, M. Owczarek, S. J. Lee, J. W. Choi and J. F. Stoddart, *Nat. Energy*, 2019, **4**, 51–59.